

Implementation of the Joint-Unscented Kalman Filter for Online
Characterization of Synchronous Machines

A Thesis

Presented in Partial Fulfilment of the Requirements for the

Degree of Master of Science

with a

Major in Electrical Engineering

in the

College of Graduate Studies

University of Idaho

by

Andrew Miles

Major Professor: Brian K. Johnson, Ph.D.

Committee Members: Eric Wolbrecht, Ph.D.; Joseph Law, Ph.D.

Department Administrator: Mohsen Guizani, Ph.D.

May 2017

Authorization to Submit Thesis

This thesis of Andrew Miles, submitted for the degree of Master of Science with a major in Electrical Engineering and titled “Implementation of the Joint-Unscented Kalman Filter for Online Characterization of Synchronous Machines,” has been reviewed in final form. Permission, as indicated by the signatures and dates given below, is now granted to submit final copies to the College of Graduate Studies for approval.

Major
Professor: _____ Date: _____
Brian K. Johnson, Ph.D.

Committee
Members: _____ Date: _____
Eric Wolbrecht, Ph.D.

Joseph Law, Ph.D.

Department
Administrator: _____ Date: _____
Mohsen Guizani, Ph.D.

Abstract

As the capacity of power systems worldwide is growing, the need for accurate equipment models to keep the grid stable has increased. When installing new generation equipment, nameplate data will be provided by the contractors to be recorded and documented. Currently, there is a shift to include as much renewable energy generation sources as possible. However, to incorporate these facilities into the modern power system, detailed studies are needed to realize benefits of the new generation. Due to the need for an accurate model of the power system, the WECC and NERC introduced a new policy which states that utilities need to maintain up to date parameters for their systems. Consequently, the common practice is to follow the IEEE 115 standard which requires that the generator is taken offline. Taking a generator offline creates an enormous cost for the generation facility due to the time required to parameterize the machines, so revenue is lost.

To regain revenue where possible, methods to parameterize machine while they are online have been explored. This thesis explores algorithms and advises ways to parameterize a generator while it is online. The Joint-Unscented Kalman Filter was chosen to capture the states and estimate the parameters of a salient pole synchronous machine while it is online. The chosen filter algorithm was tested, tuned, and verified against a simulated generator. Furthermore, the Joint-Unscented Kalman filter algorithm was tested on a physical laboratory setup and was compared against IEEE 115 tests conducted on the machine, providing promising results toward further industrial implementation.

Acknowledgements

I thank my major professor, Dr. Brian K. Johnson for his valuable time and insightful suggestion throughout completing my thesis. I'm also thankful to Dr. Eric Wolbrecht, and Dr. Joseph D. Law for their valuable time and suggestion which motivated, and assisted me along the progress of my work.

Special thanks to Dr. Normann Fischer and Schweitzer Engineering Laboratories for sponsoring this work.

I am also thankful to Mr. Michael West, for assisting me as I was introduced to the research project to further studies on this research. I am also thankful to my fellow students of the ECE department who have been part of my Masters's Degree Completion.

Dedication

This work is dedicated to my mother, Judy, for her absolute love and encouragement. To my sister Kimberly for her support, and to friends for their camaraderie throughout my personal and academic life. Without them, I would not be where I am today without their motivation and support.

Table of Contents

Authorization to Submit Thesis	ii
Abstract	iii
Acknowledgements	iv
Dedication	v
Table of Contents	vi
Tables	xi
Figures	xii
Acronyms	xiv
Nomenclature	xv
Chapter 1: Introduction	1
1.1 Background and Motivation.....	1
1.2 Literature Review	2
1.2.1 Offline Characterization.....	2
1.2.2 Online Characterization	3
1.2.2.1 Black Box Method	3
1.2.2.2 White Box Method.....	4
1.2.2.3 Gray Box Method.....	4
1.2.3 Chosen Method	5
1.3 Scope of the Thesis	6
1.4 Summary	6
Chapter 2: Synchronous Machine Modelling	7
2.1 Synchronous Machine ABC Domain.....	7
2.2 DQ Reference Frame.....	9

2.3	Park's Transformation: DQ0.....	10
2.4	Flux Linkage	11
2.5	State Space Equations	14
2.5.1	6 th Order State Space Equations.....	16
2.5.2	4 th Order State Space Equations.....	16
2.6	Summary	17
Chapter 3:	Unscented Kalman Filter Theory.....	18
3.1	Unscented Kalman Filter.....	18
3.1.1	Terms.....	18
3.2	Unscented Kalman Filter Algorithm.....	19
3.2.1	Overview of Operation.....	19
3.2.1.1	Initialization Step at k=0	21
3.2.1.2	Prediction Update.....	22
3.2.1.3	Measurement Update	22
3.3	Joint Unscented Kalman Filter Algorithm	23
3.3.1	State Space	23
3.3.2	Summary	25
Chapter 4:	MATLAB Test System	26
4.1	The Test System.....	26
4.1.1	Simulink Model.....	26
4.1.1.1	Synchronous Generator	28
4.1.1.2	Transformer Parameters	29
4.2	Measurement in Simulink	29
Chapter 5:	MATLAB Machine Simulations and State Estimation Results.....	31

5.1	Simulation Technique	31
5.1.1	Steady State	31
5.1.2	Transient Test.....	33
5.1.2.1	Three Phase Fault.....	33
5.1.2.2	Step Load	33
5.2	Steady State Model Verification	35
5.2.1	Steady State Objective	35
5.2.2	Steady State Gains.....	35
5.2.3	Steady State Test Results	36
5.3	Transient State Model Verification	42
5.3.1	Transient Gains	43
5.3.2	Transient State Test Results	44
5.4	Summary	50
Chapter 6:	Lab Generator Testing Analysis and Results	51
6.1	Lab Setup	51
6.1.1	Generator	51
6.2	Measurement Requirements.....	52
6.2.1	Time Alignment of Encoder to Data	53
6.3	Offline Parameter Estimation.....	53
6.3.1	Parameterization of X_d	54
6.3.2	Parameterization of X_q	54
6.3.3	Parameterization of X_0	55
6.3.4	Parameterization of L_{ls}	56
6.3.5	Parameterization of L_{md}	56

6.3.6	Parameterization of L_{mq}	57
6.3.7	Final Offline Machine Parameters	57
6.4	Test Description	57
6.4.1	Initialization	58
6.4.2	Loaded Condition Test.....	58
6.5	Results	59
6.6	Summary	62
Chapter 7:	Sensitivity Analysis.....	64
7.1	Noise	64
7.2	Data Sampling	65
7.3	Time Alignment	66
7.3.1	Sample Rate	67
7.4	Power Factor Control	68
7.5	Torque Measurements	69
7.6	Summary	69
Chapter 8:	Conclusion and Future Scope.....	71
8.1	Conclusion.....	71
8.2	Future Work	73
References	76
Appendix A – Characteristics	78
Open Circuit Characteristics	78
Synchronous Condenser Operation to Calculate X_q Data.....	79	
Appendix B – AMPS Setup	81
Variable Frequency Drive	81	

Encoder	81
Current Transformer.....	81
SEL-411L Relay Settings.....	81
SEL-735 Relay Settings	82
Analog Model Power System	84
Synchronization to the Power Grid.....	84

Tables

TABLE 1: PARAMETERS FOUND FROM THE IEEE 115 STANDARD [2].....	2
TABLE 2: 187 MVA SYNCHRONOUS GENERATOR PARAMETERS [18]	28
TABLE 3: 187 MVA TRANSFORMER PARAMETERS.....	29
TABLE 4: STEADY STATE KALMAN FILTER GAINS	36
TABLE 5: STEADY STATE PARAMETER RUNS	42
TABLE 6: TRANSIENT KALMAN FILTER GAINS	44
TABLE 7: TRANSIENT PARAMETER ESTIMATION	49
TABLE 8: 20 HORSEPOWER SYNCHRONOUS GENERATOR NAME PLATE DATA	52
TABLE 9: SYNCHRONOUS GENERATOR CALCULATED BASE VALUES	52
TABLE 10: FINAL OFFLINE MACHINE PARAMETERS.....	57
TABLE 11: SAMPLE SHIFT DISTRIBUTION OF VOLTAGES AND CURRENTS SAMPLED AT 8 KHZ AT 0.85 PF.....	59
TABLE 12: GENERATOR OPERATING POINT AT 0.85 PF LEADING	60
TABLE 13: PARAMETER DISTRIBUTION AT 8 KHZ AS SAMPLE SHIFT VARIED.....	61
TABLE 14: VOLTAGE AND CURRENT DISTRIBUTION AT 30.72 KHZ WITH 0.83 PF LEADING AS SAMPLE SHIFT VARIES	61
TABLE 15: PARAMETER DISTRIBUTION AT 30.72 KHZ WITH 0.83 PF LEADING	62
TABLE 16: FINAL PARAMETERS FOR THE 20 HORSEPOWER SYNCHRONOUS MACHINE AT 8 KHZ AND 30.72 KHZ .	63
TABLE 17: PERCENT ERROR OF THE PARAMETERS FOUND AT 8 KHZ AND 30.72 KHZ	63

Figures

FIGURE 1: MODEL TYPE FLOW CHART	5
FIGURE 2: DQ0 REFERENCE FRAME DIAGRAM	9
FIGURE 3: DQ0 TRANSFORM OF A SYNCHRONOUS MACHINE WITH TWO Q-AXIS DAMPER WINDINGS [8]	14
FIGURE 4: UNSCENTED KALMAN FILTER OPERATION	25
FIGURE 5: MODIFIED POWER_TURBINE MODEL IN SIMULINK INCLUDING OUTPUTS [15].....	27
FIGURE 6: STATE ESTIMATION OF THE D-AXIS AND Q-AXIS FLUXES	37
FIGURE 7: STATE ESTIMATION OF THE 0-AXIS AND KQ1-AXIS FLUXES	38
FIGURE 8: STATE ESTIMATION OF THE FIELD AND KD -AXIS FLUXES	38
FIGURE 9: MEASUREMENT ESTIMATION OF OMEGA AND DELTA OF THE MACHINE	39
FIGURE 10: MEASUREMENT ESTIMATION OF THE SYSTEM D -AXIS AND Q-AXIS CURRENTS	39
FIGURE 11: MEASUREMENT ESTIMATION OF THE SYSTEM 0-AXIS AND FIELD CURRENTS	40
FIGURE 12: ESTIMATION OF L_{MD} AND L_{MQ}	41
FIGURE 13: ESTIMATION OF $LLFD$ AND LLS	41
FIGURE 14: STATE ESTIMATIONS FOR D-AXIS, AND Q-AXIS FLUXES	45
FIGURE 15: STATE ESTIMATION OF THE 0-AXIS AND KQ AXIS FLUXES	45
FIGURE 16: STATE ESTIMATION OF THE FIELD AND DK-AXIS FLUXES.....	46
FIGURE 17: MEASUREMENT ESTIMATION AND VERIFICATION OF SYSTEM MEASUREMENTS OMEGA AND DELTA ..	46
FIGURE 18: MEASUREMENT ESTIMATIONS OF THE SYSTEM CURRENTS I_Q AND I_D	47
FIGURE 19: MEASUREMENT ESTIMATIONS OF THE SYSTEM CURRENTS I_0 AND I_{FIELD}	47
FIGURE 20: L_{LKQ} AND L_{LKD} ESTIMATION	48
FIGURE 21: R_{KQ} AND R_D ESTIMATION	48
FIGURE 22: LAB 20 HORSEPOWER SYNCHRONOUS GENERATOR.....	51
FIGURE 23: PHASOR DIAGRAM OF A SALIENT POLE SYNCHRONOUS GENERATOR.....	55
FIGURE 24: RAW VS FILTERED DATA (A) CURRENT (B) VOLTAGE	65
FIGURE 25: POWER SYSTEM MEASUREMENTS ON MARCH 14, 2017, AT 1 PM TO 4 PM.	69
FIGURE 26: CONNECTION PANEL NEXT TO 20 HP SYNCHRONOUS GENERATOR	84
FIGURE 27: CONNECTION PANEL ON AMPS SYSTEM ABOVE COMPUTER.....	85

FIGURE 28: GENERATOR BUS CONFIGURATION..... 85

FIGURE 29: BREAKER BOX FOR AMPS MG SET 86

FIGURE 30: SYNCHROSCOPE..... 87

Acronyms

3PH – Three Phase Fault

IEEE – Institute of Electrical and Electronic Engineers

UKF – Unscented Kalman Filter

NERC – North American Electric Reliability Corporation

RMS – Root-Mean-Square

VFD – Variable Frequency Drive

Nomenclature

Fluxes

λ_a - A phase flux linkage

λ_b - B phase flux linkage

λ_c - C phase flux linkage

λ_f - Excitation (field) flux linkage

λ_{d_s} - Direct axis winding flux linkage referred to the stator

λ_{q_s} - Quadrature axis flux linkage referred to the stator

λ_{fd_s} - Excitation (field) winding flux linkage referred to the stator

λ_{md} - Mutual Direct axis winding flux linkage

λ_{mq} - Mutual Quadrature axis winding flux linkage

λ_{kD_s} - Direct axis damper winding flux linkage referred to the stator

λ_{kQ_s} - Quadrature axis damper winding flux linkage referred to the stator

Inductances

L_{aa} - A to A phase self inductance

L_{ab} - A to B phase mutual inductance

L_{ac} - A to C phase mutual inductance

L_{bb} - B to B phase self inductance

L_{ba} - B to A phase mutual inductance

L_{bc} - B to C phase mutual inductance

L_{cc} - C to C phase self inductance

L_{ca} - C to A phase mutual inductance

L_{cb} - C to B phase mutual inductance

- L_{ff} - Excitation field to field self inductance
- L_{af} - A to excitation field mutual inductance
- L_{bf} - B to excitation field mutual inductance
- L_{cf} - C to excitation field mutual inductance
- L_{kDkD} - Direct axis damper winding self inductance
- L_{kDa} - Direct axis damper winding to A phase mutual inductance
- L_{kDb} - Direct axis damper winding to B phase mutual inductance
- L_{kDc} - Direct axis damper winding to C phase mutual inductance
- L_{kDkQ} - Direct axis damper winding to Quadrature axis winding mutual inductance
- L_{kQkQ} - Quadrature axis damper winding self inductance
- L_{kQa} - Quadrature axis damper winding to A mutual inductance
- L_{kQb} - Quadrature axis damper winding to B mutual inductance
- L_{kQc} - Quadrature axis damper winding to C mutual inductance
- L_{kQf} - Quadrature axis damper winding to excitation (field) axis winding mutual inductance
- L_{kQkD} - Quadrature axis damper winding to Direct axis damper winding mutual inductance
- L_{mq} - Quadrature axis magnetizing flux linkage
- L_{md} - Direct axis magnetizing flux linkage

Resistances

r_s - Resistance of stator winding, same for phases a,b,c

r_n - Stator neutral point to ground resistance

r_{kQ} - Resistance of the q axis damper winding

r_{fd} - Resistance of the field winding

r_{kD} - Resistance of the d-axis damper winding

Currents and Voltages

i_a - A phase current

i_b - B phase current

i_c - C phase current

i_{kD} - Direct axis damper winding current

i_{kQ} - Quadrature axis damper winding current

v_a - A phase voltage

v_b - B phase voltage

v_c - C phase voltage

v_f - Excitation (field) voltage

v_{kD} - Direct axis damper winding voltage

v_{kQ} - Quadrature axis damper winding voltage

v_{kD} - Direct axis damper winding voltage

v_n - Neutral Voltage

DQ0 Currents

i_d - Direct axis current

i_q - Quadrature axis current

i_0 - zero sequence current

DQ0 Voltages

v_d - Direct axis voltage

v_q - Quadrature axis voltage

V_0 - Zero sequence voltage

DQ0 Inductance

L_d - Direct axis inductance

L_q - Quadrature axis inductance

L_n - Stator neutral point to ground inductance

L_{mq} - Magnetizing inductance in the q axis

L_{md} - Magnetizing inductance in the d axis

L_{ls} - Leakage inductance in the stator winding

L_{lfd} - Leakage inductance in the field winding

L_{lkQ} - Leakage inductance in the q axis damper winding

L_{lkD} - Leakage inductance in the d axis damper winding

Chapter 1: Introduction

Every year, the demand for energy has increased. With the advent of renewable resources such as wind, solar, and tidal power the requirement for an accurate representation of the power system has also increased. Due to the increased need for an accurate model of the power system, the WECC has imposed a new policy in which generators over 20 MW need to be parameterized [1]. However, the access to a generator for parameter measurement poses a problem.

In industry, technicians use the IEEE 115 standard [2] to parametrize machines. The IEEE 115 standard provides a thorough process to gather all recommended parameters of a machine to create a suitable model. However, the IEEE 115 standard requires that the machine is taken offline to perform the tests. Taking a machine offline at a generation facility poses a problem not only in the cost of the test but in the revenue lost while the machine is offline. The total cost can vary from a smaller amount to a very large amount depending on how critical the machine is to the facility. As stated by the previous student on this project, Michael West, an estimation of the machines parameters while the machine is online can be made through a numerical algorithm to avoid taking the machine offline.

1.1 Background and Motivation

With the advent of the WECC and NERC standards, power utility companies are required to parameterize their bulk system components. This includes machines, transformers, lines and other apparatus. However, these items are taken offline to gather the proper parameters as not to affect the power system by the testing. This costs a significant amount of capital and time. Since the focus of this thesis is on machine testing, the references to tests used in industry is the IEEE 115 standard. In this standard, a machine is taken offline to be tested. When a machine is taken offline for parameterization or maintenance, it costs the company hundreds of thousands

of dollars. The motivation for this research is finding a way to avoid removing a generator from service and gather the proper parameters required by the IEEE for system modeling.

1.2 Literature Review

In this section, the various ways to parameterize a synchronous generator are explored to provide a review. The IEEE 115 standard is discussed for offline parameterization, and why the application of the standard poses a problem for current utilities. Online parameterization techniques are explored; furthermore, an algorithm for online parameterization is chosen.

1.2.1 Offline Characterization

In industry, the current standard for parameterizing a synchronous machine for modeling is the IEEE 115 standard [2]. This extensive testing procedure takes days to complete; however, it provides a confident procedure for engineers to follow to obtain the proper parameters. The tests and parameters to be found from the IEEE 115 standard are listed in Table 1.

Table 1: Parameters found from the IEEE 115 Standard [2]

Test	Parameters to Be Found
Open Circuit	Open Circuit Curve
Short Circuit	Short Circuit Saturation Curve
Slip Test	X_{qs}, X_{qw}, X_{ds}
Applied Negative Sequence Current	X_2, R_2
Series Circuit	X_0, R_0
Sudden Short Circuit	$X'_d, X''_d, \tau'_d, \tau''_d$

As shown above, the IEEE 115 guidelines allow the industry to gather all parameters from a synchronous machine. From the slip test parameters, such as the direct-axis reactance X_{ds} and

quadrature-axis reactances X_{qs} and X_{qu} are calculated. Negative sequence reactance and resistance, X_2 and R_2 , calculated from the negative sequence current injection test. The zero-sequence reactance and resistance, X_0, R_0 , calculated from the series circuit test. Lastly, the direct-axis subtransient and transient reactances and time constants, $X'_d, X''_d, \tau'_d, \tau''_d$, may be calculated from the sudden short circuit test on the synchronous machine. However, the IEEE 115 standard requires that the test machine be taken offline, which may pose problems for a facility wishing to gain revenue from the specific machine.

1.2.2 Online Characterization

Through an online characterization method, a utility may parametrize their machine without invasive testing. Secondly, through an algorithmic approach, the parameters of a synchronous machine may be found without taking the machine offline or stopping it. Algorithms come in a variety of applications and are determined by how they process the data. Such models are described in the following subsections:

1.2.2.1 Black Box Method

A black box method is a technique where the internal structure and functionalities of the box, $h(t)$, are not needed, as shown in Figure 1. This method aims to check if the software or hardware models the fundamental aspects of the system. The black box requires inputs, and then processes the data and gives a respective output. This output allows the user to determine if the performance matches what is expected. For simplicity, the black box method is the easiest to make as it only focuses on inputs and outputs. However, the black box method is not suitable for this application as both the states and parameters of the machine need to be updated. [3][4]

1.2.2.2 White Box Method

The white box method is the other side of the black box, where the user is concerned with the functionality of the internal structure. The white box testing can uncover implementation errors in the structure of the system by analyzing the internal workings and structure. For example, if applied to software, since each line of code is accessible, an analysis of the application can be made to improve the functionality of the code. However, this is only applicable after a given input to compare to a certain result. Then the user may check to see if the code produces the correct results [3][5].

1.2.2.3 Gray Box Method

The gray box method combines parts of both the black and white box testing. This means that the user may give input to the system, check if the model produces a correct result, and check the process in which the results were obtained. One main benefit of this method is that it provides the possibility of “intelligent” structure in which the code can test all functionalities and scenarios per both its inputs and outputs. This allows the gray box method not only to check inputs or outputs but modify the internal parameters of the system to match the inputs and outputs [3].

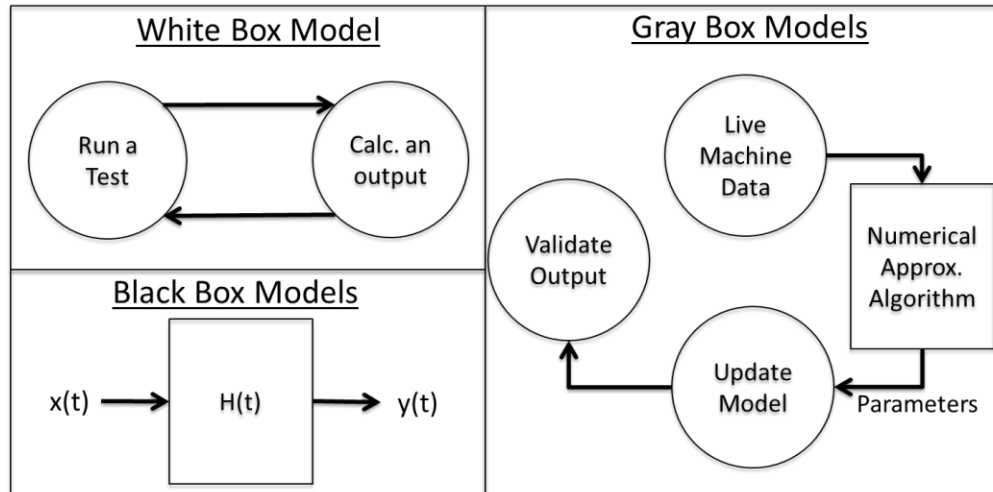


Figure 1: Model Type Flow Chart

1.2.3 Chosen Method

An online parameterization of a synchronous machine requires a gray box method since both the states and parameters will need to be calculated and updated. An algorithm with the ability to perform these sets of calculations and updates must be selected. The previous researcher on this project, Michael West [6], chose the least squares approximation. The option that was chosen for this thesis is the Kalman filtering method since the options relating to the least squares approximation have already been explored on this project. However, since the traditional Kalman filter applies to linear systems, the selection of a Kalman filter variant suitable for a non-linear application was required. There are various non-linear formats of the Kalman filter, which will be discussed later. Through exploring journals and papers, it was concluded that the Unscented Kalman Filter would be used for the analysis of a synchronous generator for this thesis.

1.3 Scope of the Thesis

The objective of this thesis is the application, design, and implementation of an Unscented Kalman filter for machine parameterization. In this, it will be shown that the filter can be used to parameterize a salient pole synchronous machine. This will be demonstrated through verification against a known model in MATLAB allowing the accuracy of the filter to be assessed. Following the successful implementation of the filter in a simulation environment, this method will be applied to a physical laboratory environment and used to parameterize a physical machine.

1.4 Summary

This chapter has provided a brief insight into the current machine parameterization scenario and how current practices are being used. The principles of machine parameterization were discussed, and possible solutions were suggested. The scope of this thesis was set based on the significance of machine parameterization for accurate and reliable models of the power system.

Chapter 2: Synchronous Machine Modelling

This chapter will describe the modeling synchronous generators, more explicitly, salient pole synchronous generators. The discussion will begin with modeling the machine in the ABC domain. Next, the synchronous DQ0 reference frame will be discussed in detail. Finally, the creation of different state space models and their applications will also be derived and discussed.

2.1 Synchronous Machine ABC Domain

For a three phase, synchronous machine, the first option to study the machine is in the ABC domain. The important components of a three-phase synchronous machine are the three phases: A – Phase, B- Phase, and C-Phase windings as shown in the flux linkage equation found in (1).

$$\begin{bmatrix} \lambda_a \\ \lambda_b \\ \lambda_c \\ \lambda_f \end{bmatrix} = \begin{bmatrix} L_{aa} & L_{ab} & L_{ac} & L_{af} \\ L_{ba} & L_{bb} & L_{bc} & L_{bf} \\ L_{ca} & L_{cb} & L_{cc} & L_{cf} \\ L_{fa} & L_{fb} & L_{fc} & L_{ff} \end{bmatrix} \begin{bmatrix} i_a \\ i_b \\ i_c \\ i_f \end{bmatrix} \quad (1)$$

The inductance matrix in (1) is expanded into equations (2) through (10). Where L_{a1} is the winding leakage inductance. L_{aa0} is the inductance corresponding to the constant component of the air-gap permeance. L_{g2} is the magnitude of inductance which corresponds to the air-gap permeance that varies with rotor angle. Lastly, θ_{me} is the electrical rotor angle between the rotor direct axis and stator phase-a axis.

Stator-to-stator mutual inductances

$$L_{aa} = L_{a1} + L_{aa0} + L_{g2} \cos 2\theta_{me} \quad (2)$$

$$L_{bb} = L_{a1} + L_{aa0} + L_{g2} \cos(2\theta_{me} + 120^\circ) \quad (3)$$

$$L_{cc} = L_{a1} + L_{aa0} + L_{g2} \cos(2\theta_{me} - 120^\circ) \quad (4)$$

Stator-to-rotor mutual inductances

$$L_{af} = L_{fa} = L_{af} \cos 2\theta_{me} \quad (5)$$

$$L_{bf} = L_{fb} = L_{af} \cos(2\theta_{me} - 120^\circ) \quad (6)$$

$$L_{cf} = L_{fc} = L_{af} \cos(2\theta_{me} + 120^\circ) \quad (7)$$

Stator-to-stator mutual inductances

$$L_{ab} = L_{ba} = -\frac{1}{2} L_{aa0} + L_{g2} \cos(2\theta_{me} - 120^\circ) \quad (8)$$

$$L_{bc} = L_{cb} = -\frac{1}{2} L_{aa0} + L_{g2} \cos 2\theta_{me} \quad (9)$$

$$L_{ac} = L_{ca} = -\frac{1}{2} L_{aa0} + L_{g2} \cos(2\theta_{me} + 120^\circ) \quad (10)$$

From the inductance equations, a definition may now be made for a state space of the machine.

$$\begin{bmatrix} v_a \\ v_b \\ v_c \\ v_{fd} \\ v_{kD} \\ v_{kQ} \end{bmatrix} = \begin{bmatrix} R_a & 0 & 0 & 0 & 0 & 0 \\ 0 & R_b & 0 & 0 & 0 & 0 \\ 0 & 0 & R_c & 0 & 0 & 0 \\ 0 & 0 & 0 & R_{fd} & 0 & 0 \\ 0 & 0 & 0 & 0 & R_{kD} & 0 \\ 0 & 0 & 0 & 0 & 0 & R_{kQ} \end{bmatrix} \begin{bmatrix} i_a \\ i_b \\ i_c \\ i_{fd} \\ i_{kD} \\ i_{kQ} \end{bmatrix} - \begin{bmatrix} \dot{\lambda}_a \\ \dot{\lambda}_b \\ \dot{\lambda}_c \\ \dot{\lambda}_{fd} \\ \dot{\lambda}_{kD} \\ \dot{\lambda}_{kQ} \end{bmatrix} \quad (11)$$

In the equations (2) - (10), it is important to note the mutual dependence between each of the phases of the machine and stator to rotor dependences. Secondly, note the dependence on a cosine term within the inductance equations which introduces a time varying nonlinearity. Because of these coupled non-linear terms, machine analysis

becomes difficult. Through the machine equations, a state space representation can be created for analysis. However, all the inductances are mutually coupled and have non-linear time-varying behavior, which complicates state space analyses.

2.2 DQ Reference Frame

As seen in the previous section, the ABC domain machine equations include a lot of non-linear mutually coupled values. However, there are additional analysis techniques to decouple and transform the machine to create for equations that are easier to work with. In the case of machine analysis, transforming to a rotating DQ0 domain provides a way to decouple the ABC domain into manageable equations and remove the time variation.

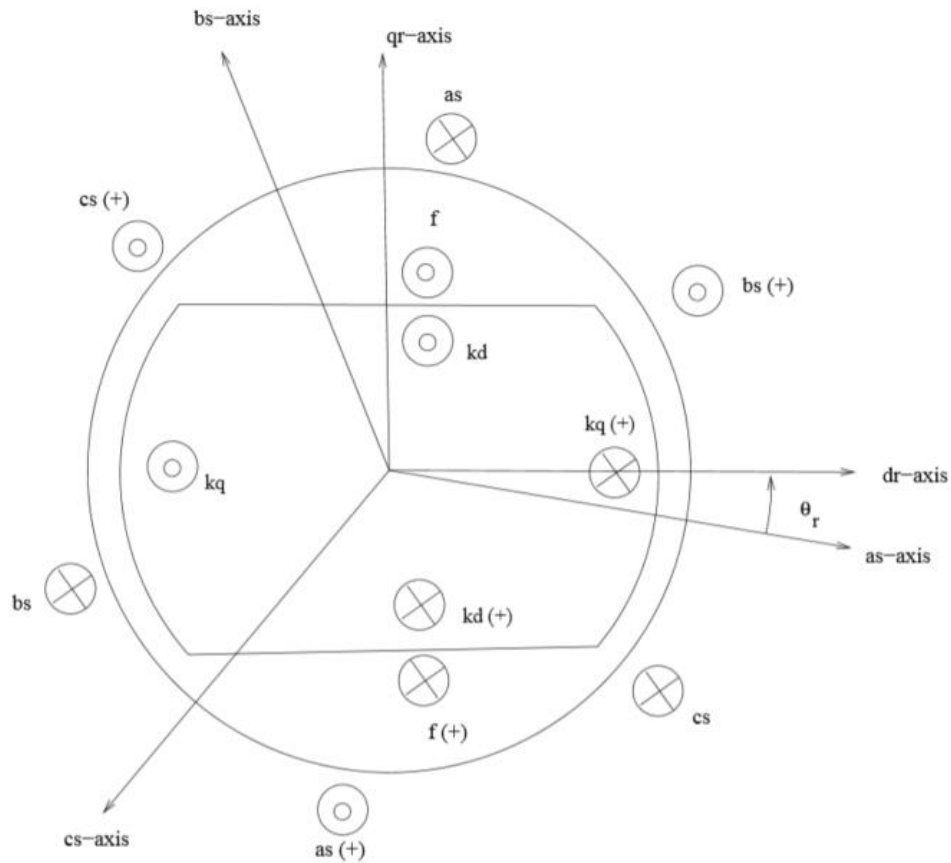


Figure 2: DQ0 Reference Frame Diagram

Figure 2 illustrates a diagram relating the ABC and DQ0 reference frames. Where the Direct axis (d-axis) is aligned with the A-phase voltage, and along the pole face of the rotor. The Quadrature axis (q-axis) is shifted from the d-axis. In this case, the q-axis leads the d-axis by 90 deg. It is important to note the rotation of the reference frame for DQ0 domain, which is described by the representation of θ_r (12). Where θ_r is the angular position of the reference frame in electrical radians which is equal to the angular position of the rotor as it turns, in electrical radians.

$$\theta_r = \omega_s t + \delta - \pi/2 \quad (12)$$

2.3 Park's Transformation: DQ0

To transform the synchronous machine equations from the ABC domain to the rotating DQ0 domain, a series of equations must be applied. Equation (13) includes the basic equation to transform to the DQ0 domain.

$$f_{dq0} = R(\theta_r)T(0)f_{abc} \quad (13)$$

$$T(0) = \frac{2}{3} \begin{bmatrix} 1 & \frac{-1}{2} & \frac{-1}{2} \\ 0 & \frac{\sqrt{3}}{2} & -\frac{\sqrt{3}}{2} \\ \frac{1}{2} & \frac{1}{2} & \frac{1}{2} \end{bmatrix} \text{ ABC to Two Axis Stationary Reference Frame} \quad (14)$$

$$R(\theta_r) = \begin{bmatrix} \cos(\theta_r) & \sin(\theta_r) & 0 \\ -\sin(\theta_r) & \cos(\theta_r) & 0 \\ 0 & 0 & 1 \end{bmatrix} \text{ Two Axis Stationary Rotating Frame} \quad (15)$$

$$T(\theta_r) = R(\theta_r)T(0) \quad (16)$$

$$f_{dq0} = T(\theta_r)f_{abc} \quad (17)$$

The set of ABC values described by f_{abc} is multiplied by the abc to two axis stationary reference frame transformation matrix (14) and then transformed to the rotating reference frame using (15). This rotating reference frame can either be synchronous with an external system, or with the rotor, or even to any stationary reference. This thesis will use the synchronous reference frame, such that $\theta_r = \omega_s t$ as seen in equation (12). The combined transform is shown in (18) is also known as “Parks Transform” [7]. By using this, an analysis of the machine can be made largely using linear state space methods.

$$\begin{bmatrix} f_{ds} \\ f_{qs} \\ f_0 \end{bmatrix} = k \begin{bmatrix} \cos(\theta_r) & \cos(\theta_r - 120^\circ) & \cos(\theta_r + 120^\circ) \\ -\sin(\theta_r) & -\sin(\theta_r - 120^\circ) & -\sin(\theta_r + 120^\circ) \\ 1/2 & 1/2 & 1/2 \end{bmatrix} \begin{bmatrix} f_{as} \\ f_{bs} \\ f_{cs} \end{bmatrix} \quad (18)$$

Where $k = \frac{2}{3}$ (19)

The application of the Parks Transform, (20) – (21) may be used to derive the voltage equations in the DQ0 domain. Where r_s is the stator resistance, i_{dq0} represents the stator currents of the machine in the DQ0 domain, p is the derivative operator, ω is the angular speed in rad/s, and λ_{dq0} are the DQ0 fluxes.

$$T(\theta_r)v_{abc} = r_s T(\theta_r)i_{abc} + T(\theta_r)p\lambda_{abc} \quad (20)$$

$$v_{dq0} = r_s i_{dq0} + p\lambda_{dq0} + \omega\lambda_{qd0} \quad (21)$$

2.4 Flux Linkage

Now that the ABC domain equations have been decoupled to the DQ0 domain, the inductances are independent of time and frequency as seen in (22) – (27). Since the inductances are now reduced, the voltages and currents in the DQ0 domain may also be determined as seen in (28) – (41). A special note are the mutual inductance terms L_{aq} (34) and L_{ad} (35) which are the

inductances combined in parallel to their respected axis. These terms are calculated values used in the calculation of the mutual flux λ_{mq} (36) and λ_{md} (37). It is important that the mutual inductances are all the inductances in parallel. With the DQ0 domain equations, a circuit may be configured as shown in Figure 3. This circuit is subject to change depending on the configuration of the synchronous machine. These changes are related to how many damper bars the synchronous machine has in each axis.

$$L_d = (L_{ls} + L_{md}) \quad (22)$$

$$L_q = (L_{ls} + L_{mq}) \quad (23)$$

$$L_{FD} = (L_{lFD} + L_{md}) \quad (24)$$

$$L_{kQ1} = (L_{lkQ1} + L_{mq}) \quad (25)$$

$$L_{kD} = (L_{lkD} + L_{md}) \quad (26)$$

$$L_0 = (L_{ls} + 3L_n) \quad (27)$$

Stator Voltage Equations:

$$V_d = p\lambda_d - \omega_r\lambda_q - r_s i_d \quad (28)$$

$$V_q = p\lambda_q + \omega_r\lambda_d - r_s i_q \quad (29)$$

$$V_0 = p\lambda_0 - r_s i_0 \quad (30)$$

Rotor Voltage Equations:

$$v_{fd} = p\lambda_{fd} + r_{fd} i_{fd} \quad (31)$$

$$v_{kD} = 0 = p\lambda_{kD} + r_{kD} i_{kD} \quad (32)$$

$$v_{kQ} = 0 = p\lambda_{kQ} + r_{kQ}i_{kQ} \quad (33)$$

Expanded Mutual Flux Equations:

$$L_{aq} = \left(\frac{1}{L_{mq}} + \frac{1}{L_{ls}} + \frac{1}{L_{lkQ1}} + \frac{1}{L_{lkQ2}}\right)^{-1} \quad (34)$$

$$L_{ad} = \left(\frac{1}{L_{md}} + \frac{1}{L_{ls}} + \frac{1}{L_{lFD}} + \frac{1}{L_{lkD}}\right)^{-1} \quad (35)$$

$$\lambda_{mq} = L_{aq} \left(\frac{\lambda_q}{L_{ls}} + \frac{\lambda_{kQ}}{L_{lkQ1}}\right) \quad (36)$$

$$\lambda_{md} = L_{ad} \left(\frac{\lambda_d}{L_{ls}} + \frac{\lambda_{fd}}{L_{lFD}} + \frac{\lambda_{kD}}{L_{lkD}}\right) \quad (37)$$

Current Equations:

$$i_d = \frac{-1}{L_{ls}} (\lambda_{ds} - \lambda_{md}) \quad (38)$$

$$i_q = \frac{-1}{L_{ls}} (\lambda_{qs} - \lambda_{mq}) \quad (39)$$

$$i_0 = \frac{-1}{L_{ls}} L_0 \quad (40)$$

$$i_{fd} = \frac{1}{L_{lfd_s}} (\lambda_{fd_s} - \lambda_{md}) \quad (41)$$

Combining the equations above we can create the following flux linkage matrix relationship:

$$\begin{bmatrix} \lambda_d \\ \lambda_q \\ \lambda_0 \\ \lambda_{kQ} \\ \lambda_{fd} \\ \lambda_{kD} \end{bmatrix} = \begin{bmatrix} -L_d & 0 & 0 & 0 & L_{md} & L_{md} \\ 0 & -L_q & 0 & L_{mq} & 0 & 0 \\ 0 & 0 & -L_0 & 0 & 0 & 0 \\ 0 & -L_{mq} & 0 & L_{kQ1} & 0 & 0 \\ -L_{md} & 0 & 0 & 0 & L_{fd} & L_{md} \\ -L_{md} & 0 & 0 & 0 & L_{md} & L_{kD} \end{bmatrix} \begin{bmatrix} i_d \\ i_q \\ i_0 \\ i_{kQ} \\ i_{fd} \\ i_{kD} \end{bmatrix} \quad (42)$$

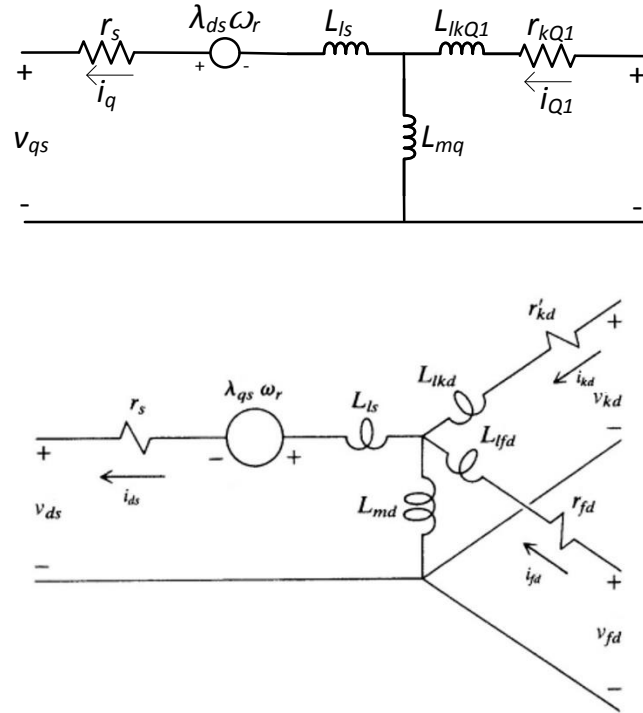


Figure 3: DQ0 transform of a synchronous machine with two Q-Axis damper windings [8]

2.5 State Space Equations

State space equations for the machine electromagnetic behavior may be determined based on the derived circuit found in Figure 3. As prescribed in [7,8,9,10] these state space equations will be the backbone of the modeling done in this thesis. Equations (43) to (46) are the d-axis, q-axis, Zero-axis, and field flux linkage differential equations respectively. The DQ0 and field axis equations will always be present in the machine modeling in this thesis, with additional equations for different scenarios. Equations (47) and (48) are the damper (amortisseur windings) windings which will only be included if the physical construction of a machine includes these windings. To fully observe the machines states, additional states and measurements must be made for the system of equations to be stable.

$$\dot{\lambda}_d = (v_d + \omega_r \lambda_q + \frac{r_s}{L_{ls}} ((\lambda_{md} - \lambda_d))) \quad (43)$$

$$\dot{\lambda}_q = (v_q - \omega_r \lambda_d + \frac{r_s}{L_{ls}} ((\lambda_{mq} - \lambda_q))) \quad (44)$$

$$\dot{\lambda}_0 = (V_0 - \frac{r_s}{L_{ls}} \lambda_0) \quad (45)$$

$$\dot{\lambda}_{fd} = (v_{fd} + \frac{r_{fd}}{L_{ifd}} ((\lambda_{md} - \lambda_{fd}))) \quad (46)$$

$$\dot{\lambda}_{kQ} = (v_{kQ} + \frac{r_{kQ}}{L_{lkQ}} ((\lambda_{mq} - \lambda_{kQ}))) \quad (47)$$

$$\dot{\lambda}_{kD} = (v_{kD} + \frac{r_{kD}}{L_{lkD}} ((\lambda_{md} - \lambda_{kD}))) \quad (48)$$

To obtain observability, the speed of the machine must also be estimated. Equation (50) represents the change in speed of the machine where J is the inertia constant. And, where T_m is the mechanical torque on the shaft of the synchronous machine which is related to power in, and T_e is the electromechanical torque produced by the machine, which is calculated using (50).

$$\dot{\omega} = \frac{1}{J} (T_m - T_e) \quad (49)$$

$$T_e = \frac{3 \text{ poles}}{2} \frac{p}{2} (\lambda_d i_q - \lambda_q i_d) \quad (50)$$

Measurements must also be made to observe the system. The measurements required are: the peak ABC voltage (L-N) and line current, field voltages, and currents, and the speed of the rotor, all sampled versus time. These measurements are required for a stable system.

2.5.1 6th Order State Space Equations

To account for damper windings in the d-axis and q-axis, additional equations are added for each respective damper winding. The 6th order set of equations in (51) accounts for one damper winding each in both the d-axis and q-axis. The 6th order model includes the effects of the damper windings during transient conditions on the machine, providing an accurate model for transient simulations. Note that 6th order means six coupled first order differential equations.

$$\begin{bmatrix} \dot{\lambda}_d \\ \dot{\lambda}_q \\ \dot{\lambda}_0 \\ \dot{\lambda}_{kQ} \\ \dot{\lambda}_{kD} \\ \dot{\lambda}_{fd} \end{bmatrix} = \begin{bmatrix} V_d + \omega_r \lambda_q + (r_s/L_s)(\lambda_{md} - \lambda_{md}) \\ V_q - \omega_r \lambda_d + (r_s/L_s)(\lambda_{mq} - \lambda_{mq}) \\ V_0 - (r_s/L_s)\lambda_0 \\ V_{kQ} + (r_{kQ}/L_{kQ})(\lambda_{mq} - \lambda_{kQ}) \\ V_{kD} + (r_{kD}/L_s)(\lambda_{md} - \lambda_{kD}) \\ V_{fd} + (r_{fd}/L_s)(\lambda_{md} - \lambda_{fd}) \end{bmatrix} \quad (51)$$

2.5.2 4th Order State Space Equations

When analyzing a machine that does not have damper windings, the state space reduces to a 4th order system. Also, the 6th order equation may also be reduced if the machine is in a steady state since the currents in the damper windings are zero. The 4th order equations allow easier analysis but are not numerically stable if the machine physically includes damper windings.

$$\begin{bmatrix} \dot{\lambda}_d \\ \dot{\lambda}_q \\ \dot{\lambda}_0 \\ \dot{\lambda}_{fd} \end{bmatrix} = \begin{bmatrix} V_d + \omega_r \lambda_q + (r_s / L_{ls})(\lambda_{md} - \lambda_{md}) \\ V_q - \omega_r \lambda_d + (r_s / L_{ls})(\lambda_{mq} - \lambda_{mq}) \\ V_0 - (r_s / L_{ls})\lambda_0 \\ V_{fd} + (r_{fd} / L_{ls})(\lambda_{md} - \lambda_{fd}) \end{bmatrix} \quad (52)$$

2.6 Summary

This chapter has explored several modeling scenarios pertinent to this thesis. The implementation of these equations through an algorithmic approach to estimate the states and parameters of a generator. Principles and equations in this chapter were used to define the model of a synchronous machine will be applied in Chapters 3 and 4.

Chapter 3: Unscented Kalman Filter Theory

3.1 Unscented Kalman Filter

The Unscented Kalman Filter (UKF), first proposed by Julier et al [12,13] and then further developed by Wan and Van der Merwe [14,15,16], was devised as an alternative to the Extended Kalman Filter (EKF). The main difference between the UKF and the EKF is that the EKF uses the Jacobian to linearize the non-linear system to achieve first order accuracy. Both the UKF and EKF use Gaussian random variables (GRV). However, because the UKF is a sigma-point filter, it uses a deterministic sampling approach to select the minimal set of chosen sample (sigma) points. Through these sample points, the UKF no longer needs a first order system linearized through the Jacobian, and can effectively capture the posterior mean and covariance of a 2nd order approximation, for any nonlinearity.

3.1.1 Terms

\tilde{x}_k^+ = *posteriori estimate of the initial state vector*

\tilde{x}_k^- = *priori state estimate*

$x_k^{(a)}$ = *augmented state matrix with states and noise*

χ_k = *vector of sigma points*

P_k^- = *error covariance*

P_{xy} = *cross covariance*

\tilde{y}_k^- = *predicted measurement*

$E(x)$ = *expected value (guess)*

$K_k = \text{Kalman gain}$

$t_k = \text{time}$

$w_k = \text{process noise}$

$v_k = \text{measurement noise}$

$Q_k = \text{covariance of process noise}$

$R_k = \text{covariance of measurement noise}$

$u_k = \text{input measurements}$

$\rho_k = \text{parameter vector}$

3.2 Unscented Kalman Filter Algorithm

3.2.1 Overview of Operation

To estimate the parameters and states of the machine, a definition of the discrete nonlinear process model must first be made [17].

$$x_k = F(x_{k-1}, u_{k-1}) + w_{k-1} \quad (53)$$

$$y_k = H(x_k, u_k) + v_k \quad (54)$$

$$w_k \sim (0, Q_k) \quad Q = \text{cov}\{w\} = E\{w * w^T\} \quad (55)$$

$$v_k \sim (0, R_k) \quad R = \text{cov}\{v\} = E\{v * v^T\} \quad (56)$$

The objective of this system is to estimate recursively x_k from the output measurements y_k . This means calculating estimates of x_k at time k , given the y_1, \dots, y_k values up to time k . Using the assumption that the initial function of the state vector $(x_0 | y_0)$ is known, $(x_k | y_k)$ is obtained

recursively in a two-step process: prediction step and update step using the non-linear equations $x = F(x)$ and $y = H(x)$ respectively. Where x_k is the state vector, u_k is the system input vector and y_k is the output vector with noise. The functions $F()$ and $H()$ are nonlinear and need to be continuous, and w_k are the process noise sequence and v_k are the observation (measurement) noise sequence to account for a noisy system. Noise is assumed to be Gaussian (normal distribution) with zero mean and known time invariant covariance matrices.

The state distribution can also be represented by Gaussian random variables, but the method used here is a minimal set of carefully chosen sample points. These points, called sigma points, completely capture the true mean and covariance of the states and are propagated through the nonlinearity. For calculating the statistics of a random variable which undergoes a nonlinear transformation we can use the unscented transformation (UT) [17].

To understand how the sigma points are calculated and distributed, consider a variable x (dimension n), which is propagated through a nonlinear function $y = f(x)$. The mean of x can be calculated by (57) and the covariance of x is calculated by (58).

$$\bar{x} = E\{x\} \quad (57)$$

$$P_x = E\{(x - \bar{x}) * (x - \bar{x})^T\} \quad (58)$$

To calculate the statistics of y , a matrix ψ of $2 * n + 1$ sigma vectors is formed per (59) to (60).

$$\chi_0 = \bar{x} \quad (59)$$

$$\chi_i = \bar{x} + \gamma(\sqrt{P_x})_i \quad i = 1, \dots, n \quad (60)$$

$$\chi_i = \bar{x} - \gamma(\sqrt{P_x})_i \quad i = n + 1, \dots, 2 * n \quad (61)$$

Where (62) is a scaling parameter and (63) depends on the constant α which determines the spread of the sigma points around the mean value \bar{x} .

$$\gamma = \sqrt{n + \lambda} \quad (62)$$

$$\lambda = \alpha^2 * (n + k_f) - n \quad (63)$$

The constant k_f is a secondary scaling parameter and is usually set to 0 for state estimation. A note can be made that is the i -th column of the matrix square root denoted by $(\sqrt{P_x})_i$, may also be described through the Cholesky factorization method. The χ_i vectors are propagated through the nonlinear function $y_i = f(\chi_k^*)$. The mean and covariance for y are approximated using a weighted sample mean and covariance of the posterior sigma points as seen below in equations (64) to (66):

$$W_0^{(m)} = \frac{\lambda}{(n+\lambda)} \quad (64)$$

$$W_0^{(c)} = \frac{\lambda}{(n+\lambda)} + (1 - \alpha^2 + \beta) \quad (65)$$

$$W_i^{(m)} = W_i^{(c)} = \frac{1}{2*(n+\lambda)} \quad i = 1, \dots, 2 * n \quad (66)$$

As stated above, the UKF filter has two main portions, the prediction step, and the update step. Below is the main UKF state estimation algorithm, with additive (zero mean) noise [17]:

3.2.1.1 Initialization Step at $k=0$

$$\text{Initial estimated state vector } \tilde{x}_0 = E\{x_0\}$$

$$\text{Initial covariance matrix } \tilde{P}_{x,0} = E\{(x_0 - \hat{x}_0) * (x_0 - \hat{x}_0)^T\}$$

Sigma point calculation for $k \geq 1$

$$\chi_k = \left[\tilde{\chi}_{k-1} \quad \tilde{\chi}_{k-1} + \gamma \left(\sqrt{\tilde{P}_{x,k-1}} \right) \quad \tilde{\chi}_{k-1} - \gamma \left(\sqrt{\tilde{P}_{x,k-1}} \right) \right] \quad (67)$$

3.2.1.2 Prediction Update

For the prediction step, a transformation of the sigma points through the state-update function (68) must be made. Then a calculation of the apriori state estimate (69) and apriori covariance (70) are made, where the weights $W_i^{(m)}$ and $W_i^{(c)}$ are defined by equations (65) and (66).

$$\chi_k^* = F(\chi_{k-1}, u_{k-1}) \quad (68)$$

$$\tilde{\chi}_k^- = \sum_{i=0}^{2n} W_i^{(m)} (\chi_k^*)_i \quad (69)$$

$$\tilde{P}_{x,k}^- = \sum_{i=0}^{2n} W_i^{(c)} ((\chi_k^*)_i - \tilde{\chi}_k^-) ((\chi_k^*)_i - \tilde{\chi}_k^-)^T + Q \quad (70)$$

3.2.1.3 Measurement Update

Similar to the predicting step, a transformation of the sigma points through the measurement-update function found in Equation (71) will be made. Then a calculation of the apriori state estimate and apriori covariance, where the weights $W_i^{(m)}$ and $W_i^{(c)}$ are calculated in (65) and (66).

$$Y_k^* = H(\chi_{k-1}, u_k). \quad (71)$$

$$\tilde{y}_k^- = \sum_{i=0}^{2n} W_i^{(m)} * (Y_k^*)_i \quad (72)$$

$$\tilde{P}_{y,k}^- = \sum_{i=0}^{2n} W_i^{(c)} * ((Y_k^*)_i - \tilde{y}_k^-) ((Y_k^*)_i - \tilde{y}_k^-)^T + R \quad (73)$$

Calculate the cross covariance

$$\tilde{P}_{x,y,k} = \sum_{i=0}^{2n} W_i^{(c)} * ((\chi_k^*)_i - \tilde{\chi}_k^-) ((Y_k^*)_i - \tilde{y}_k^-)^T \quad (74)$$

Calculate the Kalman filter gain vector:

$$K_k = \tilde{P}_{x,y,k} * (\tilde{P}_{y,k}^-)^{-1} \quad (75)$$

Finally, calculate the estimated state and the covariance by the standard Kalman filter algorithm

$$\tilde{x}_k = \tilde{x}_k^- + K_k(y_k - \tilde{y}_k^-) \quad (76)$$

$$\tilde{P}_{x,k} = \tilde{P}_{x,k}^- - K_k \tilde{P}_{y,k}^- * K_k^T \quad (77)$$

Because the UKF does not require does not require the calculation of Jacobian at each time step k , [17], the filter can be easily applied to many different scenarios. The portion of the filter that requires the most computation time is calculating the sigma points. For computational purposes, the sigma points are re-used for both the predict and measurement steps; however, the sigma points can be re-calculated for each step. This will not be done for the application in this work to reduce possible errors within the code, or computing power.

3.3 Joint Unscented Kalman Filter Algorithm

The “Joint” Unscented Kalman filter algorithm is an augmentation of the standard UKF for both parameter and state estimation. This is done by “augmenting” the states of the UKF by including both the states and parameters.

3.3.1 State Space

Originally, the standard UKF states were:

$$x_k = F(x_{k-1}, u_{k-1}) + w_{k-1}$$

$$y_k = H(x_k, u_k) + v_k$$

However, in augmenting the states, we now have: the states of the system x_{k-1} , plus the parameters to be estimated ρ_{k-1} , inputs u_{k-1} , and noise w_{k-1} and v_k .

$$x_k = F(x_{k-1}, \rho_{k-1}, u_{k-1}) + w_{k-1} \quad (78)$$

$$y_k = H(x_k, \rho_{k-1}, u_k) + v_k \quad (79)$$

A more visual example can be explained through matrices.

$$x_k^{(a)} = \begin{bmatrix} x_k \\ w_k \\ v_k \end{bmatrix} \quad (80)$$

$$\hat{x}_0^+ = \begin{bmatrix} E(x_0) \\ 0 \\ 0 \end{bmatrix} \quad (81)$$

$$P_0^+ = \begin{bmatrix} E[(x_0 - \hat{x}_0)(x_0 - \hat{x}_0)^T] & 0 & 0 \\ 0 & Q_0 & 0 \\ 0 & 0 & R_0 \end{bmatrix} \quad (82)$$

Now, as seen in (83) there is now an augmented ρ_k matrix of 1xP parameters representing the parameters to be estimated. This extends the state matrix by n states + ρ_k .

$$\hat{x}_0^0 = \begin{bmatrix} x_k \\ \rho_k \end{bmatrix} \quad (83)$$

$$x_k^{(0)} = \begin{bmatrix} \hat{x}_0^0 \\ w_k \\ v_k \end{bmatrix} \quad (84)$$

$$\hat{x}_0^0 = \begin{bmatrix} E(x_0) \\ 0 \\ 0 \end{bmatrix} \quad (85)$$

$$P_0 = \begin{bmatrix} E[(x(t_0) - \hat{x}_0)(x(t_0) - \hat{x}_0)^T] & 0 & 0 \\ 0 & Q_0 & 0 \\ 0 & 0 & R_0 \end{bmatrix} \quad (86)$$

Using the joint-UKF provides a straight forward way to estimate the parameters of a system. However, in augmenting the states with parameters, the total state vectors increase from an 8x8 matrix to a 17x17 matrix for this system. This is not a hindrance for this system; however, in larger power system modeling which includes hundreds of states, doubling or even tripling the states can lead to significant computational expense.

3.3.2 Summary

Figure 4 shows a flow chart for the operation of the unscented Kalman filter. This filter was chosen for its increased accuracy in non-linear equations while having the same processing abilities as a filter that linearizes the equations.

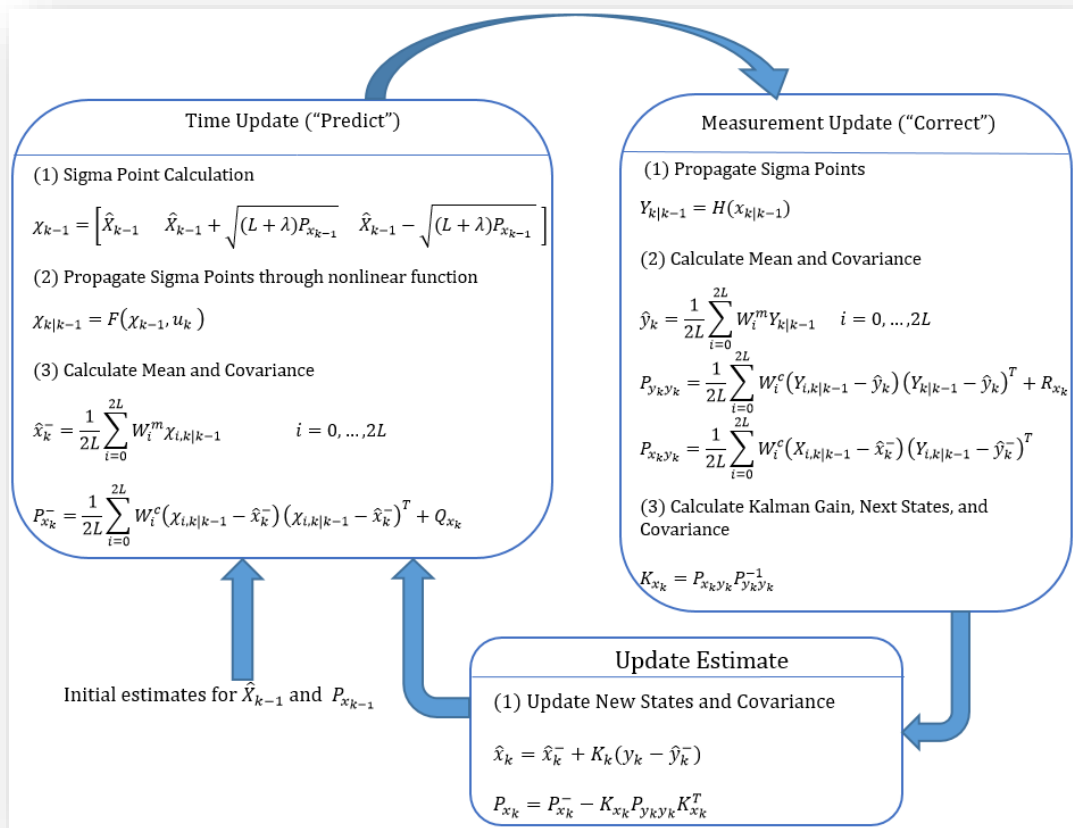


Figure 4: Unscented Kalman filter operation

Chapter 4: MATLAB Test System

4.1 The Test System

Studies were performed in the MATLAB Simulink environment [18]. The filter in its entirety was developed in code through MATLAB and then was tested against known values provided by the simpower systems add-on in Simulink. The performance of the filter was observed under the various settings, primarily: A steady state case, and a transient case to see how the filter behaved in both applications.

4.1.1 Simulink Model

To create a simulation environment which allows for fast testing, power system data was exported from Simulink to MATLAB in the form of .mat files. In Simulink, the “To File” block was used to pull required voltages, currents, and respected rotor information. Figure 5. Shows the power system setup which was analyzed in the tests. This model uses the power_turbine example as a backbone from the Simulink Library.

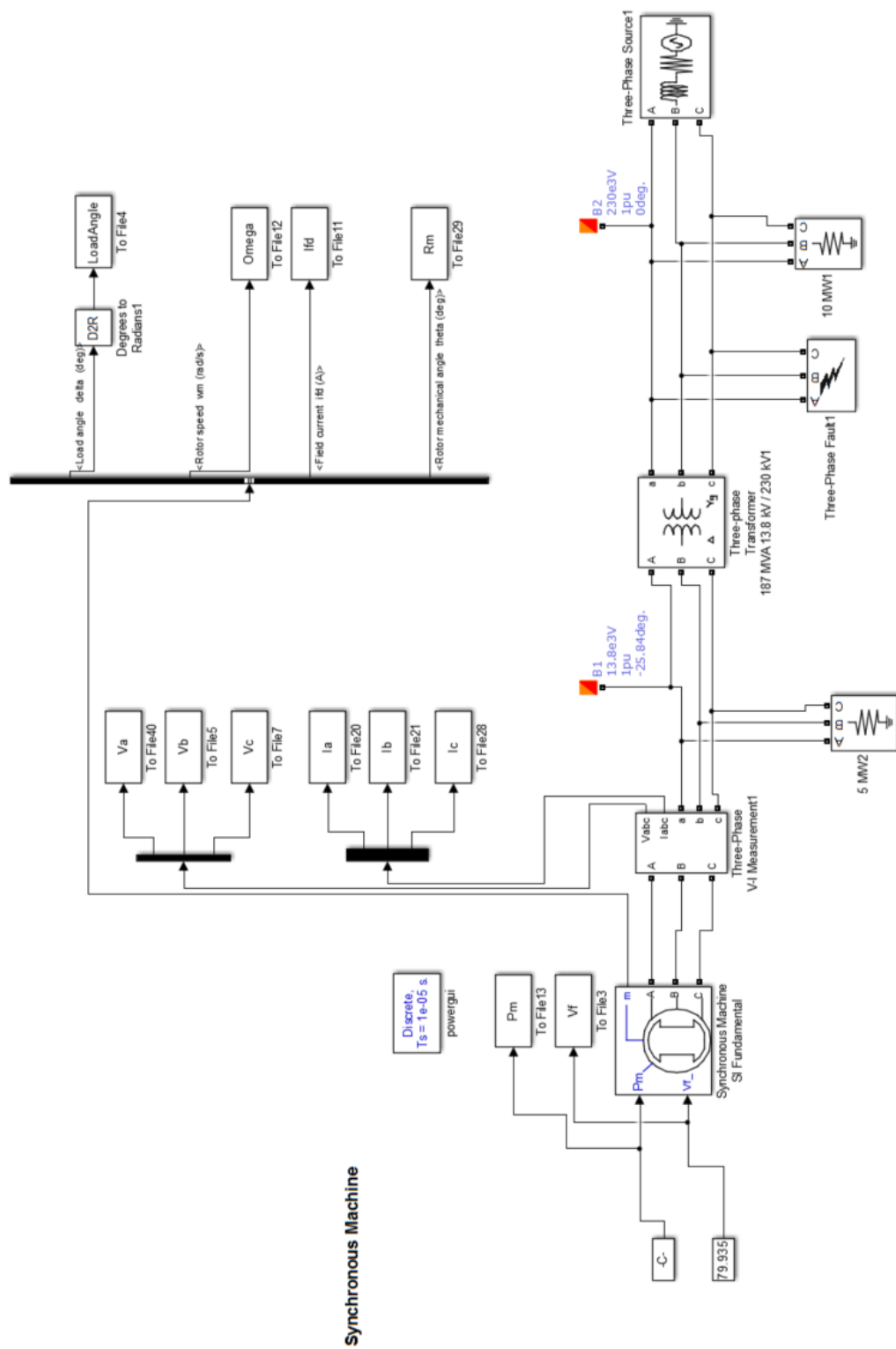


Figure 5: Modified power_turbine model in Simulink including outputs [15]

This Simulink model encompasses the generator side of the power system. Including the generation, excitation, transformer, and lines. The exciter and governor models for the generator were removed for all testing, and constant excitation and mechanical power were assumed. Due to numerical instabilities, the purely resistive load between the generator and transformer must be included in the Simulink model. This does not affect the performance of the estimation process.

4.1.1.1 Synchronous Generator

The parameters of the simulated synchronous generator are listed in Table 1. The parameter estimation algorithm will first be tested on this machine. It is important to note that an apostrophe ' is used to denote values which have been referred to the stator by the turns ratio. The 187 MVA synchronous generator block used in this parameterization was the "Synchronous machine SI fundamental" block from the power_turbine example. The generator's specific parameters can only be found within this specific block, either taken from the example, or from the default settings from the block within the library. These parameters are not included in the "pre-set model" list but are the default values when the generator is placed in the Simulink environment.

Table 2: 187 MVA Synchronous Generator Parameters [18]

Stator	L_{md}	L_{mq}	L_{ls}	r_s		
Value [H, Ohm]	3.2164E-03	9.7153E-04	3.0892E-04	2.9069E-04		
Field	Ll_{fd}'	r_{fd}'				
Value [H, Ohm]	3.0715E-04	1.9013E-03				
Damper Windings	Ll_{kq1}'	Ll_{kq2}'	r_{kq1}'	r_{kq1}'	Ll_{kD}'	r_{kD}'
Value[H, Ohm]	1.0365E-03	1.0365E-03	2.0081E-02	2.0081E-02	4.90764E-04	1.1900E-02

4.1.1.2 Transformer Parameters

The transformer used in the Simulink model is an 187 MVA Three Phase Transformer. Since the transformer in the power_turbine example comes in Per Unit, it is easy to adjust the MVA rating to match the generator.

Table 3: 187 MVA Transformer Parameters

Secondary Voltage	Primary Voltage	R1(pu)	L1(pu)	Magnetization Resistance Rm (pu)
13.8kV	230kV	0.0001	0.08	500

4.2 Measurement in Simulink

In Simulink, there are various ways to gather measurements. The method used for this application was the “send to file” block. When a simulation is run, this block creates a file in the path directory which you are testing in the MATLAB environment with that name designated on the block. These files are then called by the UKF program and read as discrete points much like values to be stored or saved in a buffer. Below are the physical measurements that are recorded for proper operation of the filter:

$$[v_{a_s}, v_{b_s}, v_{c_s}, i_{a_s}, i_{b_s}, i_{c_s}, i_{fd_s}, \omega_{rotor}, T_m, R_m]$$

Where the stator voltages $v_{a_s}, v_{b_s}, v_{c_s}$, are being recorded as peak voltage Line – Neutral. The currents are being recorded as instantaneous stator line currents denoted by $i_{a_s}, i_{b_s}, i_{c_s}$. The rotor speed ω_{rotor} is recorded in rad/s. The mechanical torque T_m into the machine is being recorded as watts. The last input required is the physical rotor position in degrees as it revolves 0 – 360

deg. For simulation purposes, a sample rate of 8 kHz was used to duplicate a sampling rate found in the power system equipment used in Chapter 7.

Chapter 5: MATLAB Machine Simulations and State Estimation Results

5.1 Simulation Technique

Through engineering judgment, it was found that approximating parameters of the machine in a two-step process greatly increases the probability of success. The first half of the estimation process incorporates the steady state operation of the machine, allowing the filter to solely estimate the steady state parameters. This is possible because while the machine is in steady state, the transient parameters cannot be estimated. The second half of the estimation process incorporates the transient parameters; however, this step also needs to incorporate the steady state values and is more efficient if the steady state values are known before the transient parameters are approximated. While successful estimation can be done with the full filter, the probability of success lies with how accurate the initial states and parameters are.

5.1.1 Steady State

The steady state test, while its primary use is for estimating states and parameters, also provides a way to initialize the filter. In removing the filter's ability to estimate the transient parameters, it will focus on estimating the steady state parameters. It is important to note that the transient states are still included in the algorithm; however, a guess of the transient parameters is only included for initialization purposes. It has been found that the transient parameters will not significantly affect the approximation of the steady state values. The initial flux calculation depends greatly on the inclusion of the fluxes in the damper windings during the initialization process. If they are not included, the filter may become unstable. In the process update section, the transient states can be "turned off" from estimation calculation. This is done by setting the transient equations to zero in the state space. Because the transient states have been set to zero, the states "freely float" to an approximated state and do not hinder the steady state calculations.

Equations (87) and (88) show the before and after state spaces with the transient parameters “turned off.” The states or parameters that are “turned off” are marked in red in (88) and will freely estimate without impacting the results of the filter.

$$\begin{bmatrix} \dot{\lambda}_d \\ \dot{\lambda}_q \\ \dot{\lambda}_0 \\ \dot{\lambda}_{kQ} \\ \dot{\lambda}_{kD} \\ \dot{\lambda}_{fd} \\ \dot{\omega} \\ \dot{L}_{md} \\ \dot{L}_{mq} \\ \dot{L}_{fd} \\ \dot{L}_{md} \end{bmatrix} = \begin{bmatrix} V_d + \omega_r \lambda_q + (r_s / L_{ls})(\lambda_{md} - \lambda_{md}) \\ V_q - \omega_r \lambda_d + (r_s / L_{ls})(\lambda_{mq} - \lambda_{mq}) \\ V_0 - (r_s / L_{ls}) \lambda_0 \\ V_{kQ} + (r_{kQ} / L_{lkQ})(\lambda_{mq} - \lambda_{kQ}) \\ V_{kD} + (r_{kD} / L_{ls})(\lambda_{md} - \lambda_{kD}) \\ V_{fd} + (r_{fd} / L_{ls})(\lambda_{md} - \lambda_{fd}) \\ (1/J)(T_m - T_e) \\ 0 \\ 0 \\ 0 \\ 0 \end{bmatrix} \quad (87)$$

$$\begin{bmatrix} \dot{\lambda}_d \\ \dot{\lambda}_q \\ \dot{\lambda}_0 \\ \dot{\lambda}_{kQ} \\ \dot{\lambda}_{kD} \\ \dot{\lambda}_{fd} \\ \dot{\omega} \\ \dot{L}_{md} \\ \dot{L}_{mq} \\ \dot{L}_{fd} \\ \dot{L}_{md} \end{bmatrix} = \begin{bmatrix} V_d + \omega_r \lambda_q + (r_s / L_{ls})(\lambda_{md} - \lambda_{md}) \\ V_q - \omega_r \lambda_d + (r_s / L_{ls})(\lambda_{mq} - \lambda_{mq}) \\ V_0 - (r_s / L_{ls}) \lambda_0 \\ 0 \\ 0 \\ V_{fd} + (r_{fd} / L_{ls})(\lambda_{md} - \lambda_{fd}) \\ 0 \\ 0 \\ 0 \\ 0 \\ 0 \end{bmatrix} \quad (88)$$

Equation (88) can be said to be a 4th order system since the only states to be estimated are the DQ0 and field states. However, the filter needs to account for flux in the damper windings and must use the full 6th order state space. Within the steady state tests, it has been assumed that prior knowledge of the stator resistance and field resistance are known or can be measured before the tests. Thus the only steady state parameters to be estimated are L_{md} , L_{mq} , Ll_{fd} and L_{ls} . Test results will be discussed in Section 5.2.

5.1.2 Transient Test

5.1.2.1 Three Phase Fault

To capture the transient parameters, the synchronous machine will need to be put through a transient condition for currents to be generated in the damper windings. It was initially stated that a three-phase fault would produce the best results and has been a common method in most papers. In simulation programs, such as Simulink one can introduce a fault onto the system easily and provide the correct measured data. However, in the physical world, it is hard to introduce a fault onto the generator terminals, let alone have a power company allow one to do so. The three-phase fault was first considered in this thesis for result verification, but will not be included in the results due to feasibility constraints.

5.1.2.2 Step Load

While the hypothetical three phase fault would be the best option, the next feasible option is one that does not require extreme operations of the generator. The ability to monitor the generator during a vigorous step load in either the form of load pickup or shedding was found from this research. If the step load is vigorous enough, it will introduce a transient condition in the machine causing a change in flux in the damper windings. The filter can now approximate the fluxes in the damper windings appropriately since the steady state parameters will have been

found before the transient condition. It is important to note that the full 6th order equations will need to be used for this approximation. For this test, a new state space and parameter selection will need to be used as seen in (89).

$$\begin{bmatrix} \dot{\lambda}_d \\ \dot{\lambda}_q \\ \dot{\lambda}_0 \\ \dot{\lambda}_{kQ} \\ \dot{\lambda}_{kD} \\ \dot{\lambda}_{fd} \\ \dot{\omega} \\ \dot{r}_{kQ} \\ \dot{L}_{lkQ} \\ \dot{r}_{kQ} \\ \dot{L}_{lkD} \end{bmatrix} = \begin{bmatrix} V_d + \omega_r \lambda_q + (r_s / L_{ls})(\lambda_{md} - \lambda_{md}) \\ V_q - \omega_r \lambda_d + (r_s / L_{ls})(\lambda_{mq} - \lambda_{mq}) \\ V_0 - (r_s / L_{ls}) \lambda_0 \\ V_{kQ} + (r_{kQ} / L_{lkQ})(\lambda_{mq} - \lambda_{kQ}) \\ V_{kD} + (r_{kD} / L_{ls})(\lambda_{md} - \lambda_{kD}) \\ V_{fd} + (r_{fd} / L_{ls})(\lambda_{md} - \lambda_{fd}) \\ (1/J)(T_m - T_e) \\ 0 \\ 0 \\ 0 \\ 0 \end{bmatrix} \quad (89)$$

As noted above, all the state equations are included; however, the steady state parameters are set as known constants and are not included in the state space. Only the transient parameters are included in the estimation process; this allows the filter to focus on just the transient parameters, increasing the likelihood of a successful estimation.

5.2 Steady State Model Verification

5.2.1 Steady State Objective

To fully observe the filters operational abilities, multiple tests were run for different input parameters. This was achieved by multiplying each initial parameter guess by a random scaling factor between +20% or -20%. Meaning, L_{md} , L_{mq} , L_{ls} , L_{lfd} , L_{lkD} , and L_{lkQ} were each multiplied by a different random percentage to re-create estimating without the exact values of the machine.

5.2.2 Steady State Gains

In determining the gains of the steady state parameter estimation calculation, it was determined that small gains for the process covariance, noise, and measurement noises provided more accurate results [19]. Table 4 to Table 6 show the respected gains recommended for steady state parameter estimation based on engineering judgment through recursive testing. The covariance matrix is comprised of the states and parameters found in (90).

$$P = \text{diag}[\lambda_d, \lambda_q, \lambda_0, \lambda_{fd}, \lambda_{kQ1}, \lambda_{kD}, \omega, L_{md}, L_{mq}, L_{lfd}, L_{ls}] \quad (90)$$

$$P_x = \text{diag}[10^{-7} \text{ Wb}, 10^{-7} \text{ Wb}, 10^{-8} \text{ Wb}, 10^{-7} \text{ Wb}, 10^{-5} \text{ W}, 10^{-5} \text{ Wb}, 10^{-6} \left(\frac{\text{rad}}{\text{s}}\right)] \quad (91)$$

$$P_p = \text{diag}[10^{-11} \text{ H}, 10^{-11} \text{ H}, 10^{-13} \text{ H}, 10^{-11} \text{ H}] \quad (92)$$

The covariance gains for the states and parameters found in (90) are explained through the series of equations in (91) and (92) where P_x is the process state covariance and P_p is the parameter covariance. Similar to the covariance matrix Q , the state and parameter process noise is described by equations (93) to (94) where Q_x is the state process noise and Q_p is the parameter process noise.

$$Q = \text{diag}[\lambda_d, \lambda_q, \lambda_0, \lambda_{fd}, \lambda_{kQ1}, \lambda_{kD}, \omega, L_{md}, L_{mq}, L_{lfa}, L_{ls}] \quad (93)$$

$$Q_x = \text{diag}[10^{-7} \text{ Wb}, 10^{-7} \text{ Wb}, 10^{-9} \text{ Wb}, 10^{-7} \text{ Wb}, 10^{-7} \text{ W}, 10^{-11} \text{ Wb}, 10^{-7} \left(\frac{\text{rad}}{\text{s}}\right)] \quad (94)$$

$$Q_p = \text{diag}[10^{-11} \text{ H}, 10^{-11} \text{ H}, 10^{-11} \text{ H}, 10^{-11} \text{ H}] \quad (95)$$

The measurement noise of the system is described by equation (96).

$$R_x = \text{diag}[10^{-7} \text{ A}, 10^{-7} \text{ A}, 10^{-9} \text{ A}, 10^{-7} \text{ A}, 10^{-7} \left(\frac{\text{rad}}{\text{s}}\right)] \quad (96)$$

Table 4: Steady State Kalman Filter Gains

	α	β	κ
Sigma Point Gains	1	2	0

It is important to note that the UKF gains for noise and covariance in Table 4 have been set loosely for steady state operation. This is to enable the filter to “search” around for the correct value. Allowing the UKF to search around avoids the possibility of finding another stable state with incorrect values. Incorrect values can be observed by knowledge of typical parameters of the stator leakage inductance L_{ls} . If L_{ls} increases or decreases down to zero or a negative value, the test will be considered null.

5.2.3 Steady State Test Results

The filter process was set up such that the final parameters were saved and exported to the workspace window. In addition to the final parameter values, plots of the states versus time, measurements, and estimated parameters were saved to verify if the filter was behaving properly. Figures 6 through 12 show the run case #3 results also summarized in Table 6. Figures 6 through 8 show the states plotted versus time. As observed, the states reach steady state after

0.2 seconds. In the case of online testing, a short convergence time is ideal, so the UKF requires fewer points to finish the estimation. An important note to make on these graphs is the scale on the y-axis as most of the graphs have an increased scale for observation purposes.

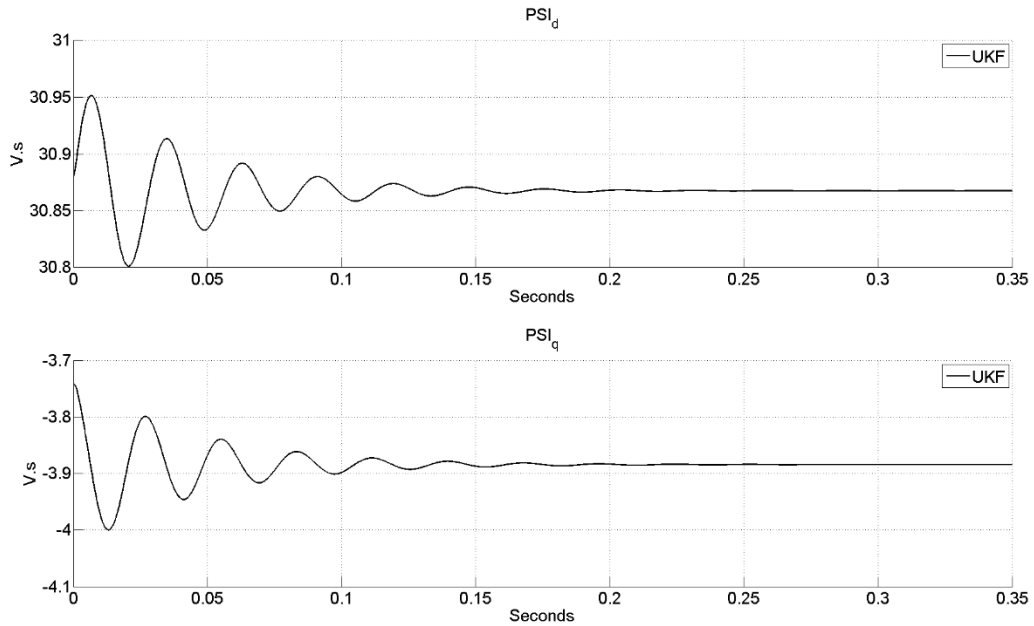


Figure 6: State estimation of the d-axis and q-axis fluxes

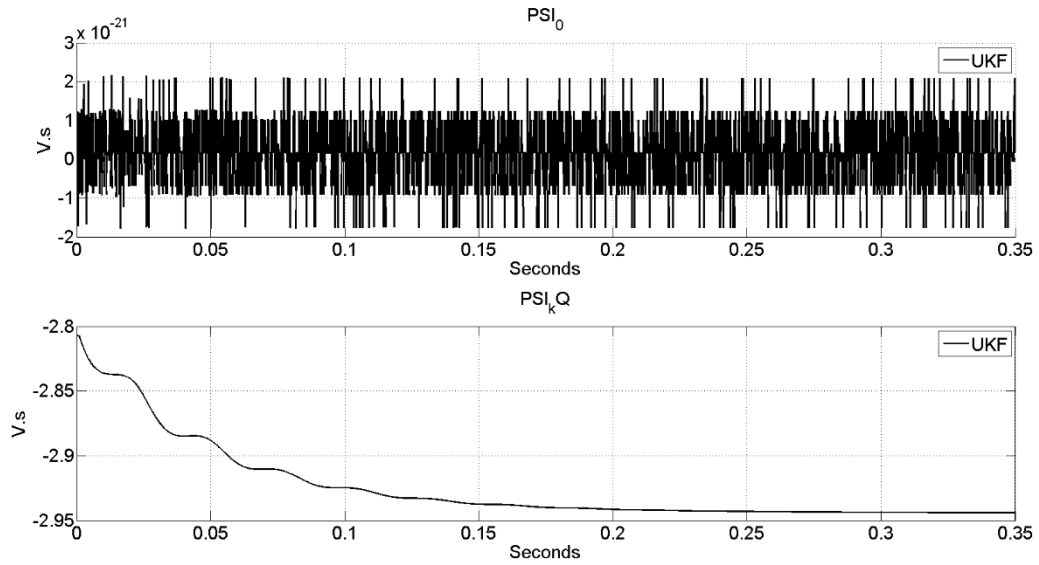


Figure 7: State estimation of the 0-axis and kQ1-axis fluxes

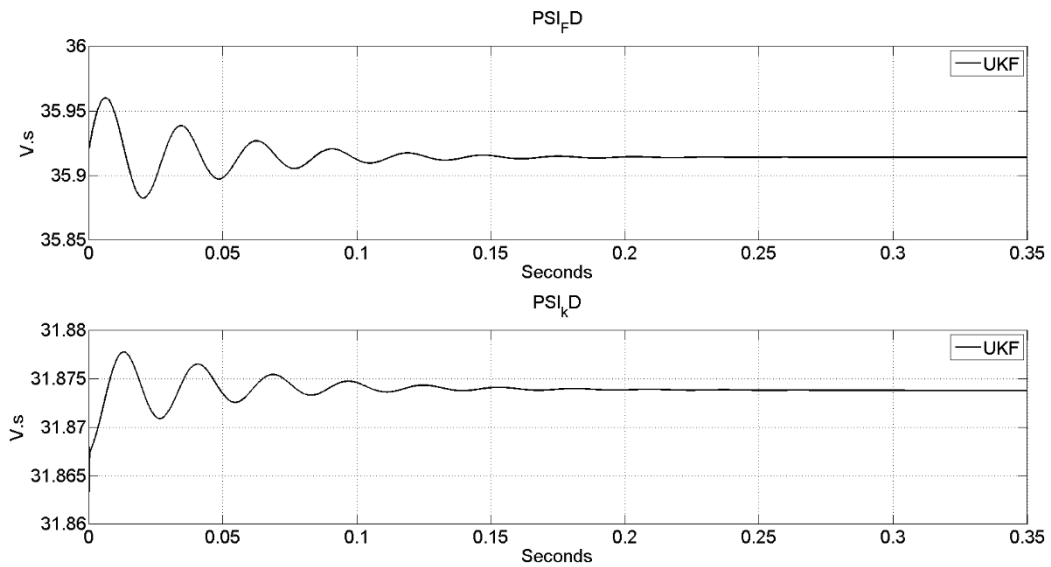


Figure 8: State estimation of the field and kD-axis fluxes

In addition to the states, the comparison of the estimated measurements with the physical measurements is a primary focus of plotting the states. If the estimated measurements are not matching the actual values known in this test case, the filter has an error or has improper gains. Figures 9 and 10 show the estimated measurements in black plotted against the actual values in

red. If it looks as if there is only one plot, the estimated value has covered the actual value. The Simulink cases are included measurements such as load angle (Δ). The load angle and mutual flux measurements were not used in the filter state space, but provided an extra calculation, check to ensure the filter has been configured properly.

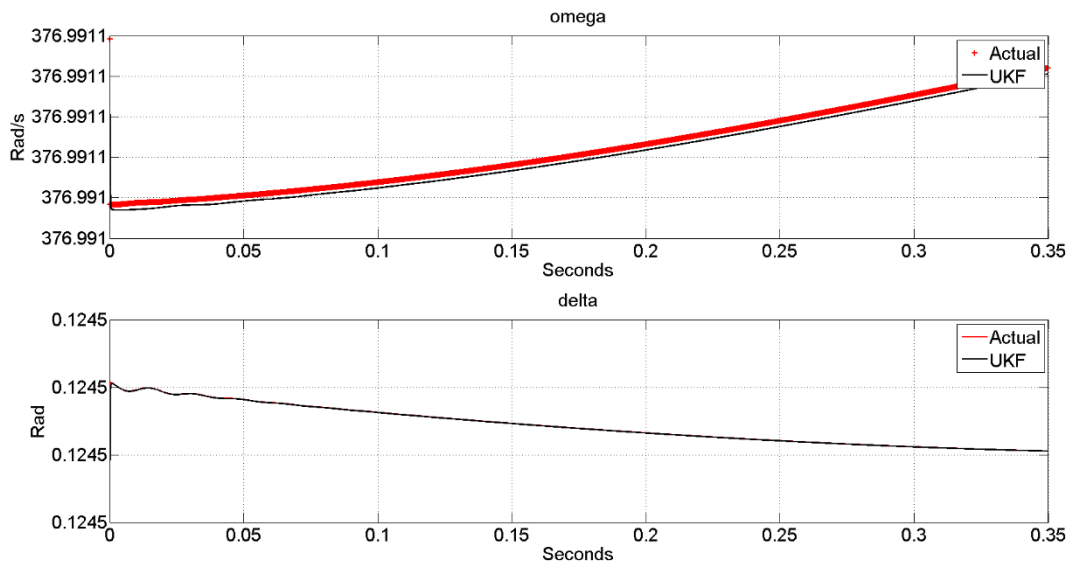


Figure 9: Measurement Estimation of omega and delta of the machine

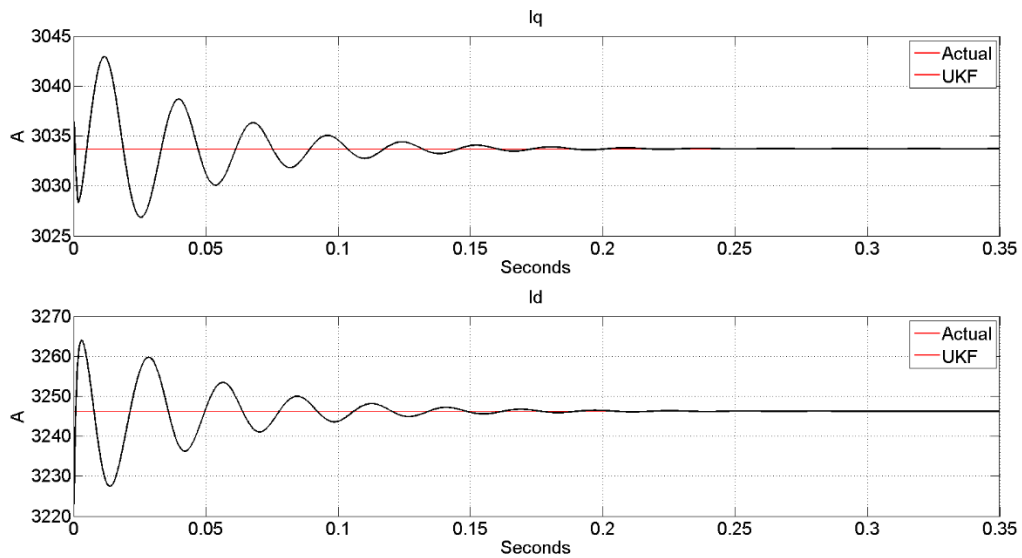


Figure 10: Measurement estimation of the system D-axis and q-axis currents

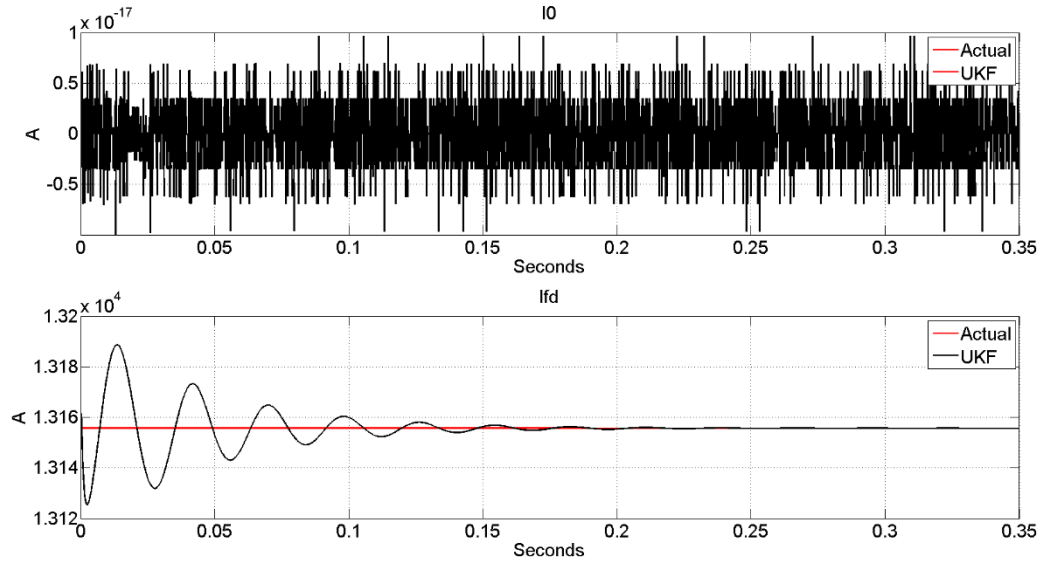


Figure 11: Measurement estimation of the system 0-axis and Field currents

The steady state parameter estimation plots of L_{md} L_{mq} and L_{ls} L_{FD} are shown in Figure 12 and 13 respectively. As noted above, the filter reaches steady state at around 0.3 seconds and will remain at this value.

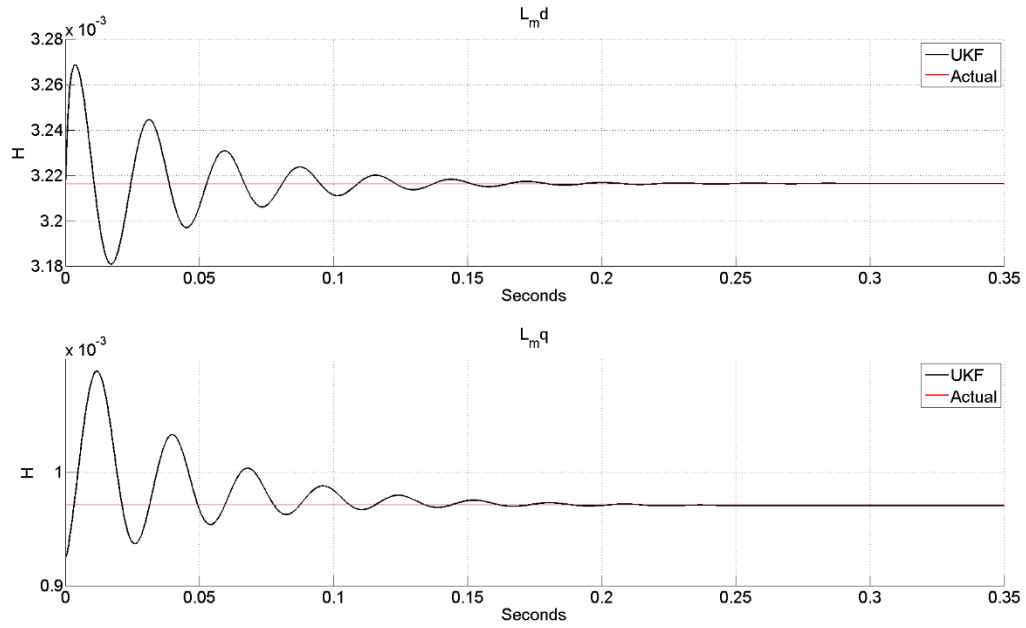


Figure 12: Estimation of $L_{m,d}$ and $L_{m,q}$

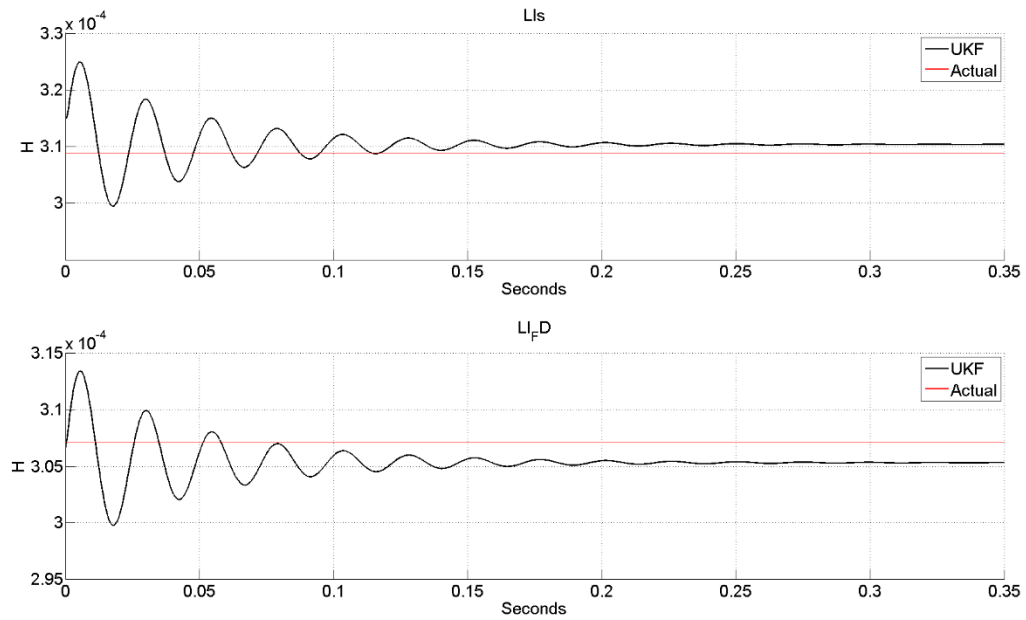


Figure 13: Estimation of L_{IFD} and L_{ls}

Table 5 summarizes the parameter estimation of three separate tests. The column “Test # Initial % Error” is the initial percent error of the parameter used for the initial guess. For example,

Run 1 Initial % error for L_{mq} was -7.2378%, meaning the initial guess value of L_{mq} was decreased by -7.2378%. The next column “Test 1 Estimated % Error” is the percent error of the final value the filter estimated.

Table 5: Steady State Parameter Runs

Variable	Actual Value	Test 1 Initial % error	Test 1 Estimated % Error	Test 2 Initial % error	Test 2 Estimated % Error	Test 3 Initial % error	Test 3 Estimated % Error
L_{md}	3.2164E-3	0.90878	-0.00313	14.512	0.099238	1.2431	-0.03455
L_{mq}	9.7153E-4	-7.2378	-0.03934	2.4962	-1.0705	-13.109	0.27821
L_{ls}	3.0712E-4	-3.7417	0.75638	3.2107	-0.9441	-6.0807	-4.9406
L_{lFD}	3.0892E-4	-0.9991	0.12478	-5.785	3.662	-6.5503	-0.3255

While the parameters of the machine are the primary focus of this work, it is also important to observe the states and measurements throughout the estimation process. While the fluxes of the machine are not observable, the currents and rotor speed are. Comparing the estimated currents and rotor speeds to the actual value provide a check of performance which can be observed in Simulink and are displayed in Figures 9 and 10.

5.3 Transient State Model Verification

To estimate the transient parameters from the synchronous machine, it must be subjected to a transient condition. This requires changing from the 4th order set of equations to a fully defined 6th order equations. Additionally, the steady state parameters L_{md} , L_{mq} , L_{ls} , L_{lFD} , r_s , and r_{fd} must be known to ensure an accurate estimate with the load pickup test. It was verified that the steady state values do not need to be known for a three-phase fault test. However, this test is not

feasible on power system equipment. Second, while the filter adjusts its covariance matrix throughout its estimation, it's advisable to use a new set of gains for a transient parameter estimation since the covariance between the points differs for a short period, rather than maintaining a steady state.

5.3.1 Transient Gains

Similar to the steady state values, the process covariance was set to a smaller value. The primary difference from the steady state case lies in the choice of noise gains. The transient process noise gain has all been increased by a factor of 10. Increasing the value of the noise gain will damp the filter in the transient period, again allowing the filter to avoid an incorrect estimation. Equation (97) describes an overview of the covariance gain for the system where each state has an individual gain. Equations (98) and (99) illustrate the matrix break down of the covariance of the process where the covariance for both the states P_x and parameters P_p are combined into one full covariance matrix.

$$P = \text{diag}[\lambda_d, \lambda_q, \lambda_0, \lambda_{fd}, \lambda_{kQ1}, \lambda_{kD}, \omega, L_{kD}, L_{kQ}, r_{kD}, r_{kQ}] \quad (97)$$

$$P_x = \text{diag}[10^{-7} \text{ Wb}, 10^{-7} \text{ Wb}, 10^{-9} \text{ Wb}, 10^{-7} \text{ Wb}, 10^{-7} \text{ W}, 10^{-11} \text{ Wb}, 10^{-7} \left(\frac{\text{rad}}{\text{s}}\right)] \quad (98)$$

$$P_p = \text{diag}[10^{-11} \text{ H}, 10^{-11} \text{ H}, 10^{-11} \text{ H}, 10^{-11} \text{ H}] \quad (99)$$

Similar to the process covariance matrix, the process noise gains are shown below first as the state covariance illustrated in (100) the parameter covariance in (101).

$$Q_x = \text{diag}[10^{-3} \text{ Wb}, 10^{-3} \text{ Wb}, 10^{-7} \text{ Wb}, 10^{-7} \text{ Wb}, 10^{-7} \text{ W}, 10^{-11} \text{ Wb}, 10^{-7} \left(\frac{\text{rad}}{\text{s}}\right)] \quad (100)$$

$$Q_p = \text{diag}[10^{-11} \text{ H}, 10^{-11} \text{ H}, 10^{-11} \text{ H}, 10^{-11} \text{ H}] \quad (101)$$

Equation (102) shows the measurement noise gains for the system. It was assumed to have a little noise in the measurements, to calibrate the filter. These gains will be recommended used for transient testing of the generator testing as the voltages and currents being recorded will be filtered before being analyzed by the filter.

$$R_x = \text{diag}[10^{-7} \text{ A}, 10^{-7} \text{ A}, 10^{-9} \text{ A}, 10^{-7} \text{ A}, 10^{-7} (\frac{\text{rad}}{\text{s}})] \quad (102)$$

The alpha term in Table 6 has been reduced to 0.3. In reducing the alpha term to a smaller value, the UKF assumes the mean is closer the specific sample point, creating a stiffer system.

Table 6: Transient Kalman Filter Gains

	α	β	κ
Sigma Point Gains	0.3	2	0

5.3.2 Transient State Test Results

In the transient test case, a load was switched into the system at 0.05 seconds, with both a real and reactive component. Changes of both real and reactive power are required such that there is current in both the d-axis and q-axis damper windings. It is advisable to pick-up a load which forces the synchronous machine to be put in a leading power factor to avoid saturation. The saturation case will be discussed in the future work section. The transient parameter estimation test cases in Simulink the governor and exciter systems were removed and applied as constant

values. In that way, a smaller load was needed. For the following figures, the recorded estimated parameters may be found in Test #1 in Table 4.

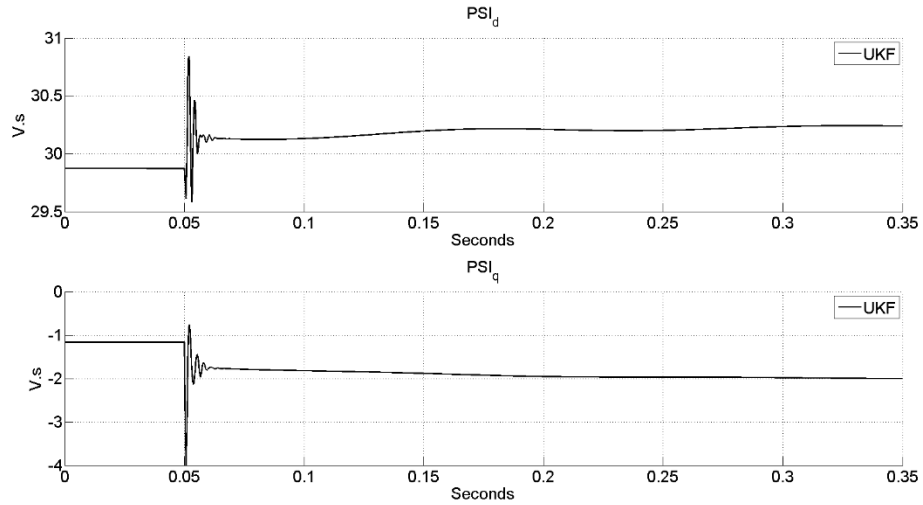


Figure 14: State estimations for d-axis, and q-axis fluxes

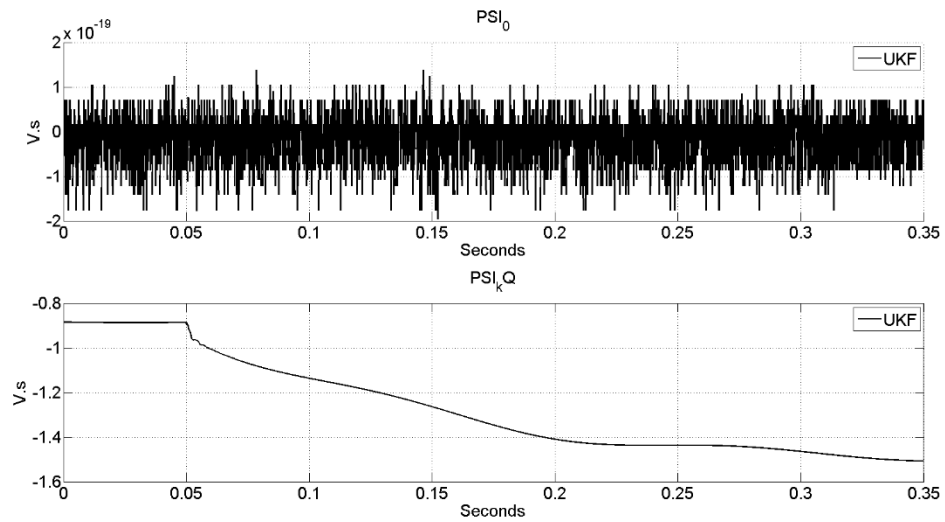


Figure 15: State Estimation of the 0-Axis and kQ axis fluxes

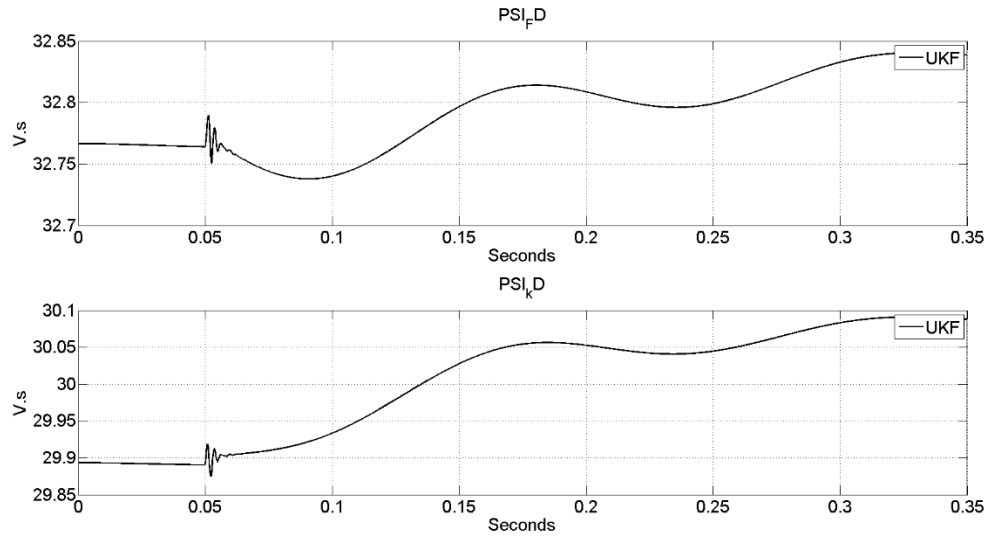


Figure 16: State Estimation of the Field and Dk-Axis fluxes

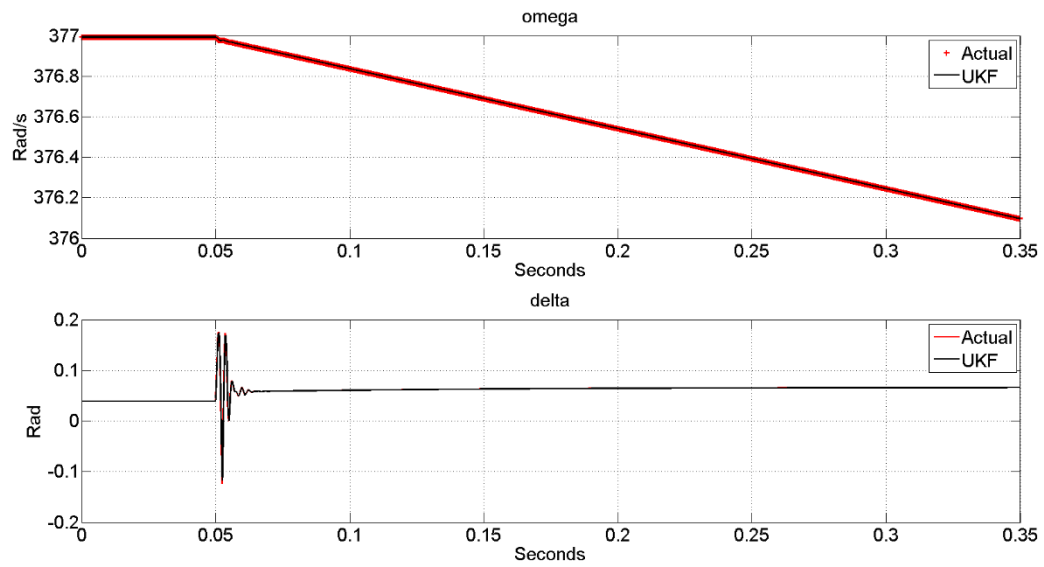


Figure 17: Measurement Estimation and verification of system measurements omega and delta

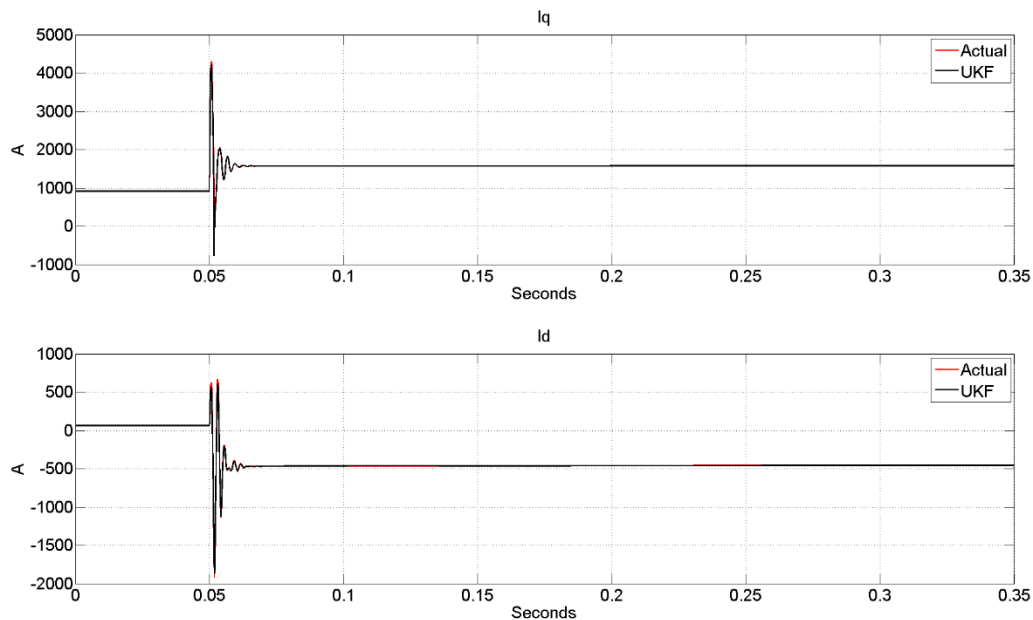


Figure 18: Measurement Estimations of the system currents I_q and I_D

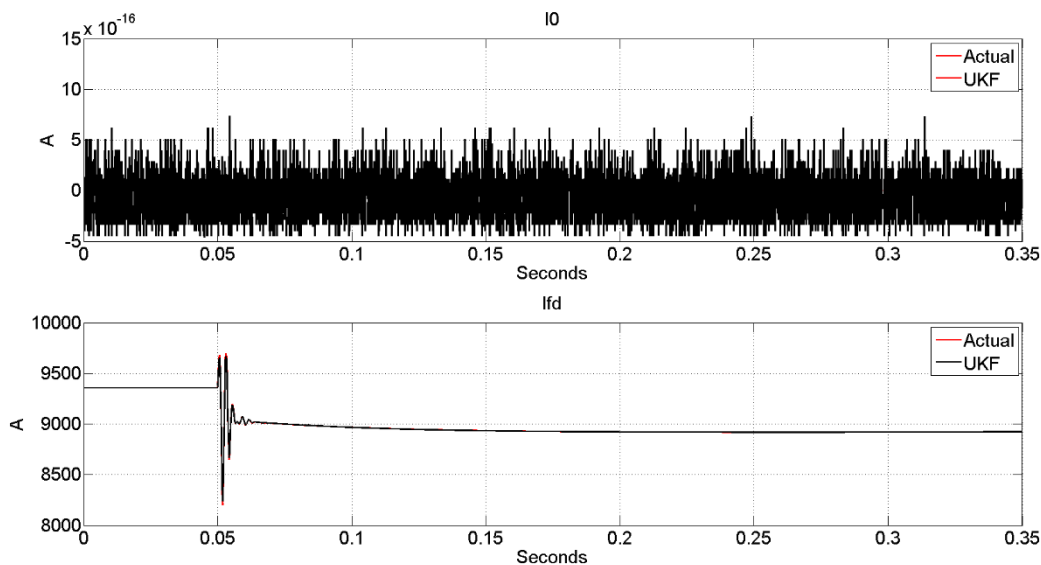


Figure 19: Measurement Estimations of the system currents I_0 and I_{field}

The transient parameter estimation plots of L_{kQ} L_{kD} and r_{kQ} r_{kD} are located below in Figures 20 and 21 respectively. As seen, the parameters reach their estimated value after 0.2 seconds similar to the steady state test conditions. The importance of these plots is the path the filter

takes to approximate the values. The filter approximates up to the proper value for L_{kQ} ; furthermore, the filter decreases its calculation to find the correct value of L_{kD} . This estimation path shows the filter has been tuned properly and converges to the correct value.

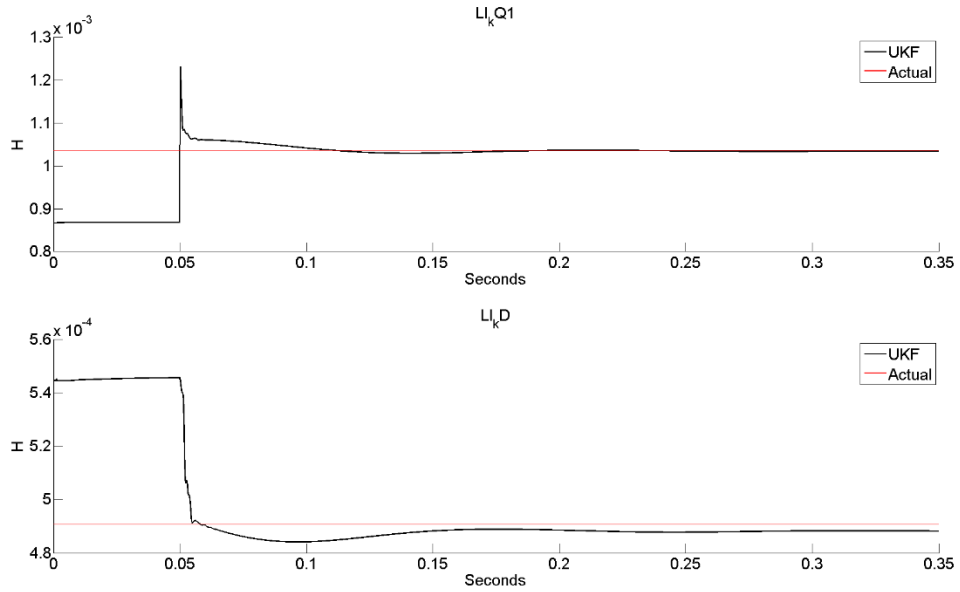


Figure 20: L_{kQ} and L_{kD} Estimation

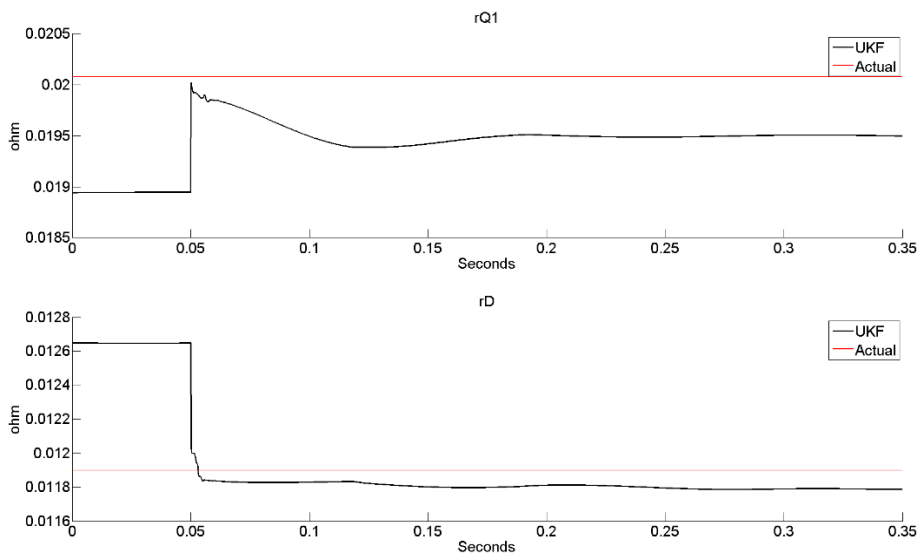


Figure 21: r_{kQ} and r_{kD} Estimation

Through numerous tests to calibrate the filter, an observation was made on a requirement for an appropriate transient parameter estimation. The filter must be able to estimate a parameter below the guessed value. Meaning, in observing Figure 20, the second plot L_{kD} decreases the initial guess value down to an approximation close to the actual value. If the gains in the filter are incorrect, the filter will only approximate to a greater value, and the results will look like a step change for all values.

Table 7 show the results of three separate runs recorded similar to the steady state tests. The column in Table 7 under “Test # Initial % Error” is the initial percent error of the parameter used for the initial guess. For example, Test 1 Initial % error for L_{kQ} was -11.11%, meaning the initial guess value of L_{kQ} was decreased by -11.11% from the known value. The next column “Test 1 Estimated % Error” is the percent error of the final value from the filter.

Table 7: Transient Parameter Estimation

Variable	Actual Value	Test 1 Initial % error	Test 1 Estimated % Error	Test 2 Initial % error	Test 2 Estimated % Error	Test 3 Initial % error	Test 3 Estimated % Error
R_{kQ} (ohm)	2.0081E-2	2.277	0.30492	7.864	1.2948	-1.528	-1.3402
L_{kQ} (H)	9.7153E-4	-11.11	2.514	-9.768	1.8756	7.9722	-0.28091
R_{kD} (ohm)	3.0712E-2	5.102	5.0895	-5.815	-4.2218	1.1206	-1.4409
L_{kD} (H)	3.0892E-4	12.634	5.3606	8.824	-3.0706	6.2661	-1.2649

5.4 Summary

As shown in Table 7, the filter approximates the parameters of the generator within 5% error. This error, however, does depend on initial guess values. One very important note about the filter operation was proper finding the proper gains for the noise and covariance. If these values are not tuned properly, the filter only approximates to a value above the initial guess; this looks like a positive step change when plotting. An observation of Figure 20 can show that while L_{Ikq} increases to the proper value, L_{IkD} decreases to its proper value. From this decrease of magnitude, it can be shown that the filter is approximating values of the generator, and not randomly finding a value determined by the additive noise.

Chapter 6: Lab Generator Testing Analysis and Results

6.1 Lab Setup

The University of Idaho has a 20 horsepower generator located in Buchanan Engineering Laboratory that is the primary focus for generator testing in this work. This generator can be synchronized to the Analog Model Power System (AMPS), which simulates a transmission system connected to the local utility system. This lab setup provides the ability to model a generator located at a facility, bringing real world challenges for parameter estimation to light within the lab.

6.1.1 Generator

The generator to be analyzed is a 20 horsepower salient pole synchronous generator shown in Figure 22. This generator's prime mover is an induction machine driven by an ABB 5550 VFD. This generator has a shaft encoder with the ability to provide the rotor angle.



Figure 22: Lab 20 horsepower Synchronous Generator

Table 8: 20 Horsepower Synchronous Generator Name Plate Data

20 Horsepower Westinghouse Salient Pole Synchronous Generator	Value
Horsepower	20
Voltage (V)	220
Current (A)	46
Field Voltage (V)	125
Power Factor	0.8
Field Current (A)	6
Frequency (Hz)	60
Poles	3

Table 9: Synchronous Generator Calculated Base Values

Calculated Generator Base	Values
Voltage Base (V)	179.63
Current Base (A)	65.0525
Field Current Base (A)	3.18
Impedance Base (Zbase) (ohm)	2.7613
Electrical Speed Base (rad/s)	376.9911

6.2 Measurement Requirements

The required measurements described in Chapter 4 have been repeated below.

$$[v_{a_s}, v_{b_s}, v_{c_s}, i_{a_s}, i_{b_s}, i_{c_s}, i_{fd_s}, R_m]$$

However, note that a couple of items have been removed. In this case, the set-up does not include a torque transducer. The mechanical torque provided to the machine must be calculated and entered the filter by hand when approximating the transient conditions of the machine.

Second, the speed of the machine must also be calculated for the transient condition of the generator as the encoder only provides rotor angle.

6.2.1 Time Alignment of Encoder to Data

The shaft encoder output is not being recorded by a relay at present and must be time aligned offline for input to the filter. In the lab, the encoder uses synchronous serial interface (SSI). This data is read from a Digilent chipKIT pro MX7. To time align the microcontroller output and the SEL-735 Relay, an output trip signal, is sent from the SEL-735 to the Digilent chipKIT pro MX7. This time aligns the microcontroller by triggering it at the same time the relay is triggered. It is important to note that the microcontroller does not record time in its data, and relies solely on the assumption that the trip sent to the microcontroller is instantaneous and without delay. The delay was found to be negligible after taking oscilloscope measurements to verify there is no time delay between the two devices.

6.3 Offline Parameter Estimation

The offline parameter estimation of the synchronous machine was produced by following the IEEE 115 Standard, as well as laboratory experiments produced from courses taught at the University of Idaho. These results are the benchmark to use for the online algorithm. The offline parameters calculated are as follows:

1. X_d
2. X_q
3. X_0

6.3.1 Parameterization of X_d

X_d was found by using the open circuit characterization analysis as followed by University of Idaho laboratory handout procedures. The machine was open circuited, and a DC voltage was applied across the field. Starting at 170V (L-L) the terminal voltage was increased in increments of 10V up to 290V. The data has been included in Appendix A.

$$X_d = \frac{V_{LN}}{\frac{I_{Field}}{\sqrt{3}} I_{SCC}} \quad (103)$$

$$X_{d1} = X_d \text{ at 1.0 Per unit voltage} \quad (104)$$

$$X_{d2} = X_d \text{ at 1.2 Per unit voltage} \quad (105)$$

$$X_d = \frac{X_{d1} + X_{d2}}{2} \quad (106)$$

$$X_d = \frac{3.740625 + 3.47969}{2} = 3.61016 \text{ ohm} \quad (107)$$

6.3.2 Parameterization of X_q

To find X_q , the machine was operated as a synchronous condenser. This allows for the q-axis to become visible since there is no real power. From Appendix B, the data can be found for X_q . The synchronous machine is now operating as a condenser, and the current produced will be in the q-axis allowing X_q to be calculated. Located below in (108) through (111) are the formulas used to calculate X_q .

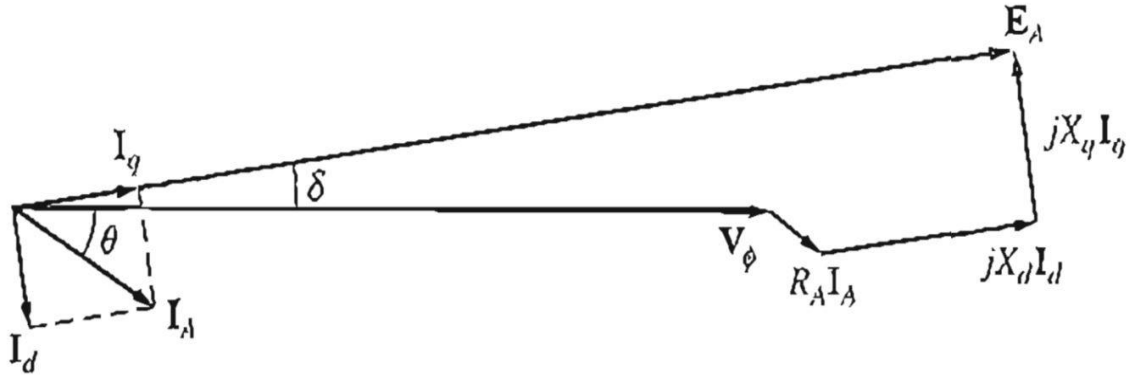


Figure 23: Phasor Diagram of a Salient Pole Synchronous Generator

$$V_{\phi} = E_A - jX_d I_d - jX_q I_q - R_A I_A \quad (108)$$

$$V_{\phi} = E_A - 0 - jX_q I_q - R_A I_A \quad (109)$$

$$X_q = \frac{V_{\phi} - E_A + I_A R_A}{j I_q} \quad (110)$$

$$X_q = 2.9577 \text{ ohm} \quad (111)$$

6.3.3 Parameterization of X_0

The test procedure for finding X_0 was based on the IEEE 115 Standard [1] for both parallel and series stator winding tests. Both tests yielded the same results, and the test data is supplied in Appendix A for reference. Once the tests were completed, equation (112) was applied to the data to find the per unit value of Z_0 , which is equivalent to X_0 . Where E in the equation is the test voltage in per unit of base line-to-neutral voltage, and I is the total test current in per unit of base current.

$$Z_0 = \frac{3E}{I} \text{ per unit} \quad (112)$$

$$Z_0 = 0.080013 \text{ Per Unit} \quad (113)$$

6.3.4 Parameterization of L_{ls}

L_{ls} cannot be directly calculated unless done through extensive testing of the machine. In the case of this study, it was assumed that X_{ls} is equal to X_0 the zero-sequence reactance. This assumption increases the amount of error in the tests; however, in the following chapter, it will be seen that it does not impact the results. To calculate L_{ls} , we need to convert X_{ls} from the per unit system to inductance in equation (115).

$$X_{ls_per.unit} = X_0_per.unit = Z_0_per.unit = 8.0013\% \quad (114)$$

$$X_{ls} = X_{ls_per.unit} Z_{base} \quad (115)$$

$$X_{ls} = 0.22094 \text{ (ohm)} \quad (116)$$

$$L_{ls} = \frac{X_{ls} Z_{base}}{\omega_{base}} \quad (117)$$

$$L_{ls} = \frac{(0.080013 \text{ (Per Unit)})(2.7613 \text{ (ohm)})}{2\pi(60\text{Hz})} \quad (118)$$

$$L_{ls} = 0.0058597 \text{ (H)} \quad (119)$$

6.3.5 Parameterization of L_{md}

L_{md} can be calculated by finding the difference between X_d and X_{ls} as shown in equation (120) through (122).

$$X_d = X_{md} + X_{ls} \quad (120)$$

$$3.65 \text{ (ohm)} = X_{md} + 0.22094 \text{ (ohm)} \quad (121)$$

$$L_{md} = \frac{3.65 \text{ (ohm)} - 0.22094}{2\pi(60\text{Hz})} = 0.0090959 \text{ (H)} \quad (122)$$

6.3.6 Parameterization of L_{mq}

The same method in calculating L_{md} can be applied for calculating L_{mq} . This may be done by finding the difference between the calculated X_q and the leakage reactance X_{ls} .

$$X_q = X_{mq} + X_{ls} \quad (123)$$

$$2.957 \text{ (ohm)} = X_{mq} + 0.22094 \text{ (ohm)} \quad (124)$$

$$L_{mq} = \frac{2.957 \text{ (ohm)} - 0.22094 \text{ (ohm)}}{2\pi(60\text{Hz})} = 0.0072162 \text{ (H)} \quad (125)$$

6.3.7 Final Offline Machine Parameters

Table 10: Final offline machine parameters

Parameter	Value
L_{md} (H)	9.0959E-3
L_{mq} (H)	7.2576E-3
L_{ls} (H)	5.8597E-4

Table 10 shows the steady-state parameters of the synchronous machine found using the IEEE 115 and University of Idaho procedures. It is important to note that the calculated values of L_{ls} and L_{l_field} are dependent on the estimation of X_0 , with the assumption that X_{ls} is similar to X_0 since a prior value of X_{ls} was not known.

6.4 Test Description

To gather the steady-state values from the synchronous machine while it is online, the synchronous machine was synchronized to the model power system and set to export power at a leading power factor. The leading power factor was chosen as it reduces the possibility of

saturation on the rotor of the synchronous machine. Procedures to synchronize to the model power system or “Grid” may be found in Appendix B. Synchronizing the synchronous machine to the grid will ensure the rotor speed of the machine is at the same frequency as the grid while the machine is loaded to export power. The first step in the test was to record the synchronous machine operation at unity power factor once the synchronous machine was synchronized to the grid. Under unity power factor, the initial reference can be calculated since delta is zero under this condition since the shaft encoder is a relative measure. Next, the prime mover (induction machine) torque was increased through the VFD, and the synchronous machine exported real power. Through excitation control, the synchronous machine put at a leading power factor to induce a current in both the d and q-axes of the machine without saturating the rotor.

6.4.1 Initialization

In the initialization step of the testing, the rotor angle of the synchronous machine must be aligned to the peak of the phase A voltage. This may only be done when the synchronous machine is at unity pf. The rotor angle “shift” with load variation will be accounted by calculating the number of samples it takes to “shift” the rotor angle zero crossing to the peak of the A-Phase voltage peak. This “shift” will be recorded in the number of samples taken and later used in the loaded condition parameter calculation.

6.4.2 Loaded Condition Test

Once the steady state initialization measurements have been recorded, the synchronous machine was set to export power by increasing the Hertz “HZ” value on the VFD. This effectively increases the torque on the shaft of the synchronous machine. Once the machine was exporting real power, the excitation control was adjusted to change the power factor of the machine to

0.85 leading. Once the pf was leading, records of the voltage, current, and rotor angle were captured. A similar sample “shift” may be calculated to find the load angle of the machine. This is achieved by again calculating the required number of samples to shift the rotor angle zero crossing to the peak of the A-Phase voltage. As a sanity check, if the machine is at a leading pf this “shift” for the loaded power factor condition should be less than the unloaded “shift” value. If the value is greater than the initial calibration sample shift, the value is incorrect. Once the rotor crossing is aligned to the A-phase peak, the difference between the unloaded condition and the loaded condition is calculated and is used to find the load angle of the machine.

6.5 Results

Following the procedure described in Section 6.4, the synchronous machine was first brought up to rated speed and synchronized to the grid. The machine voltages, currents, and field values was recorded. Next, the machine was brought to export power and 0.85 pf leading. Table 11 shows the initial distribution of operating conditions analyzed for the machine with measurements sampled at 8 kHz.

Table 11: Sample Shift Distribution of Voltages and Currents Sampled at 8 kHz at 0.85 pf

Sample Shifts	Vd (V)	Id (A)	Vq (V)	Iq (A)
0 (samples)	0.07899	-4.118	171.3	6.788
1	8.7	-3.7	171.06	6.9569
2	16.7	-3.4	170.32	7.12
2.5	20.7988	-3.186	169.8	7.2
3	24.8	-3.0	169.522	7.23
4	32.7	-2.7	168	7.41

In this test case, a shift of 2 samples was calculated after processing the data. Table 12 shows the operating condition for the generator with the machine operating at 0.85 pf leading.

Table 12: Generator Operating point at 0.85 pf leading

Test 10176	Power Factor	Sample Shift	Vd (V)	Id (A)	Vq (V)	Iq (A)
	0.85 Lead	2	16.7	-3.4	170.32	7.12

Using the recorded operational data, the parameterization of the machine was commenced. Table 13 shows a distribution of parameters approximated by the filter. As before, the calculated sample shift for this test set was two samples; however, when this data was put into the filter for estimating the parameters, the filter output became slightly unstable. This stability issue was explored, and it was concluded that the actual value for the calculated “DQ0” voltages and currents based on the angle of the q-axis (δ) approximated was halfway between to two sample shifts. This new sample shift of “2.5” as seen in Table 11 shows the dq0 voltages and currents required to keep the filter stable. Table 13 shows the estimated parameters of each sample shift. In the column named “ L_{ls} Trend” explains the trend of L_{ls} through each shift. Unstable means that L_{ls} either went to infinity or zero to keep the filter stable. When L_{ls} decreases or increases, it means that it expands to infinity or zero very slowly, and stable indicates where the filter and all its states remain stable converging to one value.

Table 13: Parameter Distribution at 8 kHz as Sample Shift Varied

Sample Shift	L_{md} (H)	L_{mq} (H)	L_{ls} (H)	L_{lfd} (H)	L_{ls} Trend
0	0.0092005	0.0064246	3.1811e-05	0.015458	Unstable
1	0.028189	0.087154	0.0013877	0.010308	Unstable
2	0.0093755	0.006581	0.00011136	0.010115	L_{ls} Decreases
2.5	0.0091415	0.0071011	0.00036287	0.009758	Stable
3	0.008928	0.0077916	0.00097494	0.010127	L_{ls} Increases
4	0.0090319	0.0095991	0.0017646	0.010124	Unstable

To test the accuracy of the parameter estimation test system, a second test set was conducted with measurements at 30.72 kHz using an SEL-735 power quality meter. The current shaft encoder is not able to sample above 20 kHz and it was sampled at 15.36 kHz then re-sampled 30.72 kHz offline. Due to the increased number of samples in the test set, a more accurate determination of the a-phase voltage peak can be made; furthermore, an accurate determination of the required sample shift (load angle) can be calculated without approximation. Table 14 shows the distribution of voltages and currents of the synchronous generator operating at 0.83 pf leading sampled at 30.72 kHz.

Table 14: Voltage and Current Distribution at 30.72 kHz with 0.83 pf Leading as Sample Shift Varies

Sample Shifts	V_d (v)	I_d (A)	V_q (v)	I_q (A)
9 (samples)	14.5091	-3.0559	129.9477	6.5755
10	16.1061	-2.975	129.7637	6.6132
11	17.6973	-2.8942	129.5662	6.6497
12	19.2907	-2.8125	129.3463	6.685
13	20.8728	-2.7309	129.1039	6.7196
14	22.4553	-2.6488	128.8438	6.7528

Table 15 shows the distribution of parameters calculated by the filter with different shifts around the original sample shift calculation of 11 samples. In these results, it is important to note that in every test case the filter estimation is stable; furthermore, all the calculated values close to the actual measured parameters from the IEEE 115 Standard test values.

Table 15: Parameter distribution at 30.72 kHz with 0.83 pf leading

Sample Shift	L_{md} (H)	L_{mq} (H)	L_{ls} (H)	L_{lfd} (H)	L_{ls} Trend
9 (samples)	0.0093376	0.0065945	0.0001097	0.010338	Stable
10	0.0091912	0.0064424	0.00021877	0.010158	Stable
11	0.0092337	0.0068743	0.00058343	0.010089	Stable
12	0.0093353	0.0069934	0.00085115	0.010087	Stable
13	0.0092703	0.0072805	0.0010599	0.01009	Stable
14	0.0094055	0.007681	0.0012452	0.010087	Stable

6.6 Summary

Tables 16 and 17 provide a comparison of the results between the two sample rates of 8 kHz and 30.72 kHz. It can be seen in Table 16 that while the 8 kHz sampling rate comes close to the IEEE 115 calculations of L_{md} and L_{mq} , the L_{ls} estimation error is quite large as noted in Table 17. It is important to note that the calculated L_{ls} for this machine was based on an estimation and not a definite value. Regardless, the estimation error with 8 kHz is still quite large due to the nature of the equations, allowing the filter to adjust L_{ls} to keep the system stable. Second, in using the 8 kHz sampling rate, the ability to verify the exact amount of samples used to calculate load angle is determined by post-processing and engineering judgment. The engineering judgment can be described as seen in Table 13 where the “correct” sample shift was 2.5 instead of 2 due to the resolution of the 8 kHz sampling of the voltages and rotor

encoder. The increased error in the 8 kHz tests is due to the inability to accurately calculate the dq0 voltages and currents of the operating point. When the filter miscalculates a sample shift by one, the filter becomes unstable and adjusts L_{ls} to keep it stable. This was the primary reason for testing at the higher 30.72 kHz sample rate as it provided the ability to remain stable even through testing ten different sample shifts on the same test. The estimation process with the 30.72 kHz sample rate does provide promising results. When the 30.72 kHz sample rate is used, the estimation errors for all values are reduced to below 5%. Note that the sample shift procedure would not have been necessary with an absolute encoder.

Table 16: Final Parameters for the 20 horsepower synchronous machine at 8 kHz and 30.72 kHz

Parameter	8 kHz samples	8 kHz 2.5 samples	30.72 kHz	Actual
L_{md} (H)	9.3755 E-3	9.1415 E-3	9.2337 E-3	9.0959E-3
L_{mq} (H)	6.581E-3	7.1011 E-3	6.9743 E-3	7.2576E-3
L_{ls} (H)	1.1136E-4	3.6287E-4	5.8343 E-4	5.8597 E-4

Table 17: Percent error of the parameters found at 8 kHz and 30.72 kHz

Parameter	8 kHz 2 Sample Error	8 kHz 2.5 Sample Error	30.72 kHz Error
L_{md} (%)	3.0739	0.50132	1.515
L_{mq} (%)	9.3226	2.1564	3.9035
L_{ls} (%)	80.996	38.074	0.43347

Chapter 7: Sensitivity Analysis

In some cases, assumptions made in simulations cannot be carried over to application of this filter to a physical system for online parameter estimation. In this section recommendations, will be made as to how to appropriately implement the UKF algorithm to estimate the fluxes and parameters of a synchronous machine.

7.1 Noise

The noise of the system depends on the type of data being recorded. In this thesis, the data was recorded using a microprocessor-based protective relay, which performed low pass filtering as part of the recording voltages and currents. This data limited the filtering which was needed to remove any harmonics, as well as measurement noise. When using raw data, the data analyzed by the UKF will need to be filtered by a low pass filter. The raw data will include noise, as well as harmonics that will need to be removed. For example, due to the construction of the 20 horsepower salient pole synchronous generator in the lab, a large 11th harmonic is observed in both the raw and filtered data, requiring the data to be filtered again. Figure 24 below provides an example of the raw data recorded plotted against the filtered quantities.

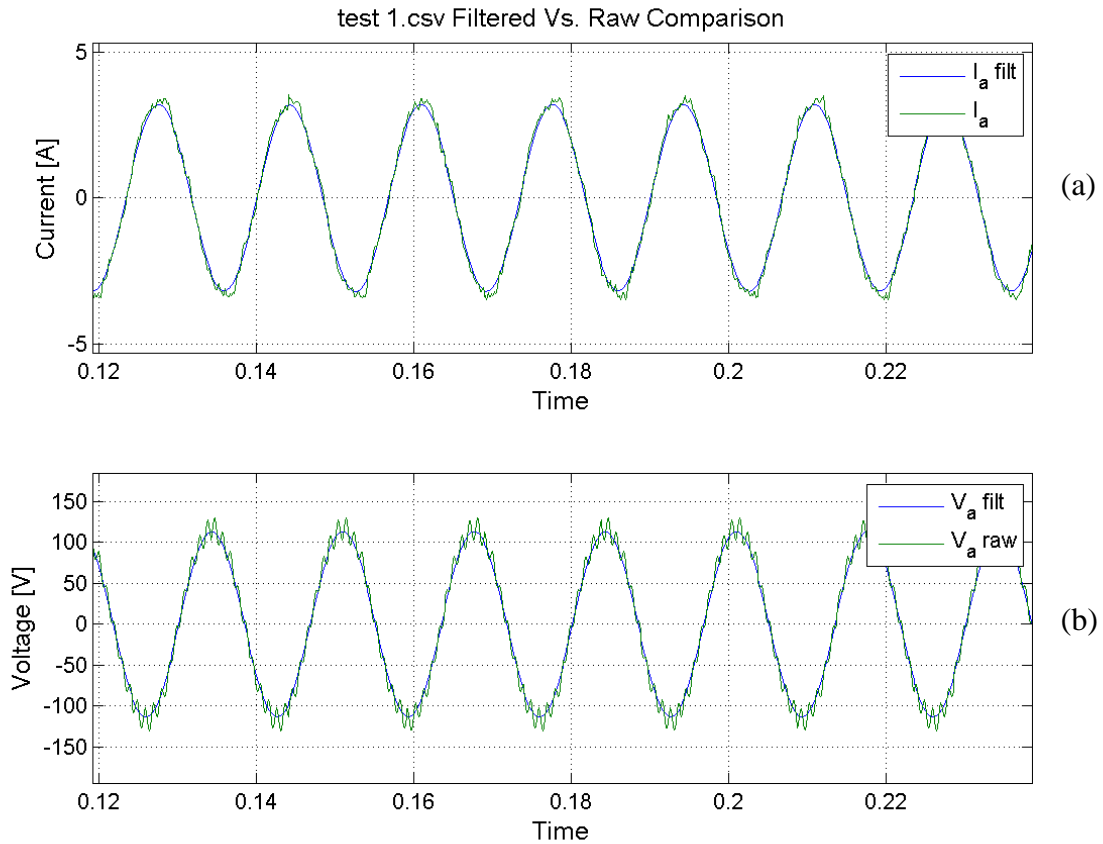


Figure 24: Raw Vs Filtered Data (a) current (b) voltage

The primary reason for filtering the voltages and currents is for increased accuracy with DQ0 analysis; furthermore, when analyzing the data offline, the filtered data provides a tangible way to accurately find the peak of the voltage for an angle reference.

7.2 Data Sampling

In this thesis, there are two main factors which surround the sample rate. Time alignment of the samples, and the sample rate itself. As discussed in Chapter 6, the sample rate impacts the estimation process and can lead to the improper estimation of parameters when using a relative encoder to determine angle. Table 16 shows the percent error from estimating with 8 kHz or 30.72 kHz rates, leading to the conclusion that 8 kHz would not be recommended. The error in

the 8 kHz values primarily stems from the ability to calculate correct voltages and currents related to the load angle of the machine. In Table 16 a sample misalignment at 8 kHz will cause an 8V shift in the d-axis voltage, causing the filter to become unstable. One sample shift error at 30.72 kHz still allows the filter to be stable; however, it does increase the error in the estimated L_{ls} value. The error in the sample shift at 30.72 kHz does again stem from the ability to calculate the actual angle of the q-axis to calculate the DQ0 voltages and currents, but the ability to calculate the correct sample shift at 30.72 kHz is simple and does not require engineering judgment in offline post-processing. A sample rate higher than 8 kHz is recommended for this application in the use of calculating an appropriate load angle of the shaft.

7.3 Time Alignment

Due to the nature of the equations used in the state and parameter estimation, the increased need for accurate time aligned samples grows especially if multiple devices are used. If the rotor quantities are not time aligned with the voltage and current measurements, it will render the analysis null. In a MATLAB simulation, the model calculates each respected value from $T = 0$, this allows for time aligned accurate values regardless of the sample rate. In a physical system, $T = 0$ is not known unless the synchronous machine has a previous rotor encoder recording of the first A-phase pole in the sequence. However, this very rare and cannot be assumed to be known.

For the laboratory experiments, a rotor encoder was installed on the synchronous machine to allow measurements of rotor position. This encoder output was recorded by a Digilent chipKIT pro MX7, rather than a microprocessor-based protective relay because the encoder uses synchronous serial interface protocol (SSI) to transmit the rotor position. Since two separate

systems are being used, the SEL-411L was used to trigger both an event report and the microcontroller at the same time.

While having the SEL-411L send a trip signal to the Digilent chipKIT pro MX7 does time align the data, the probability of error increases when there are two independent systems working in parallel. It is advised to record voltages, currents, and rotor position in one device to remove possible sources of error.

7.3.1 Sample Rate

The sample rate was the primary source of error in laboratory testing. As discussed previously, in Simulink the generator model is continuously being calculated with the discrete points recorded at a fixed sample rate. Simulink uses these discrete points for all calculations so that all calculations and measurements are aligned in space with zero error. Noise may be applied on top of these samples to increase error; however, this does not increase the error of the calculations made within the Simulink library blocks. On the physical generator, sampling the encoder to retain an accurate rotor position proved to be the primary concern.

As shown in Chapter 3, the load angle of the generator was calculated by a two-step process: the calibration step, and the loaded condition step. As seen in Table 11, at 8 kHz the voltage increases by 8 V per sample. This generates error when the filter uses the wrong value. If the filter is off by one sample shift, the calculations are now invalid, and the filter becomes unstable.

Since the SEL-411L only can sample at 8 kHz, the SEL-735 was used to sample at 30.72 kHz. The higher sampling rate of the SEL-735 allowed the error to be reduced in the voltage and current measurement; however, the rotor shaft encoder was only able to sample at 20 kHz. To ensure a consistent calculation, the encoder was only sampled at 15.36 kHz and then resampled

based on the frequency of the voltage to 30.72 kHz. The resampling of the data allowed for a higher sample rate to calculate the load angle of the machine. Tables 12 and 14 in Chapter 6 show the distribution of voltages and currents per sample for 8 kHz and 30.72 kHz. From these two tables, it can be observed that when the filter miscalculates the sample shift by one, the 8 kHz voltages and currents vary by 8 V. However, when the filter miscalculates the sample shift by one of the 30.72 kHz, it varies by 1.7 V decreasing error in the parameter estimation.

While sampling at a higher rate is promising, it is the underlying factor of load angle which determines the ability to accurately calculate the DQ0 values. The primary focus of this calculation is the A-phase voltage peak reference and the zero crossing of the rotor. If the voltage reference and rotor crossing values can be recorded with high accuracy, the need for sample rates is negligible since the rotor position can be extrapolated with the frequency of the machine. Consequently, this applies to the steady state condition of the machine as the physical rotor position will need to be recorded at a higher sample rate than 8 kHz for a transient condition as the kinematics of the rotor will need to be captured as the machine changes states.

7.4 Power Factor Control

Throughout testing the synchronous machine, it was found that without a tuned AVR the ability to keep the machine at a constant power factor depends on how rapidly the grid voltage magnitude and frequency is fluctuating. Furthermore, it has been found that during a windy day the grid voltage and frequency changes grow more dramatic and the ability to calculate a load angle becomes null. Figure 25 shows a windy day on March 14th, 2017 with samples every 3 seconds over three hours. On these days, the grid becomes inconsistent and pushes the power factor of the synchronous machine around as the machine sends a different amount of reactive power every minute. The inconsistency of the power factor on these days creates the inability

to calculate an accurate initial sample shift. The tuning of the AVR exciter is recommended to better facilitate online testing.

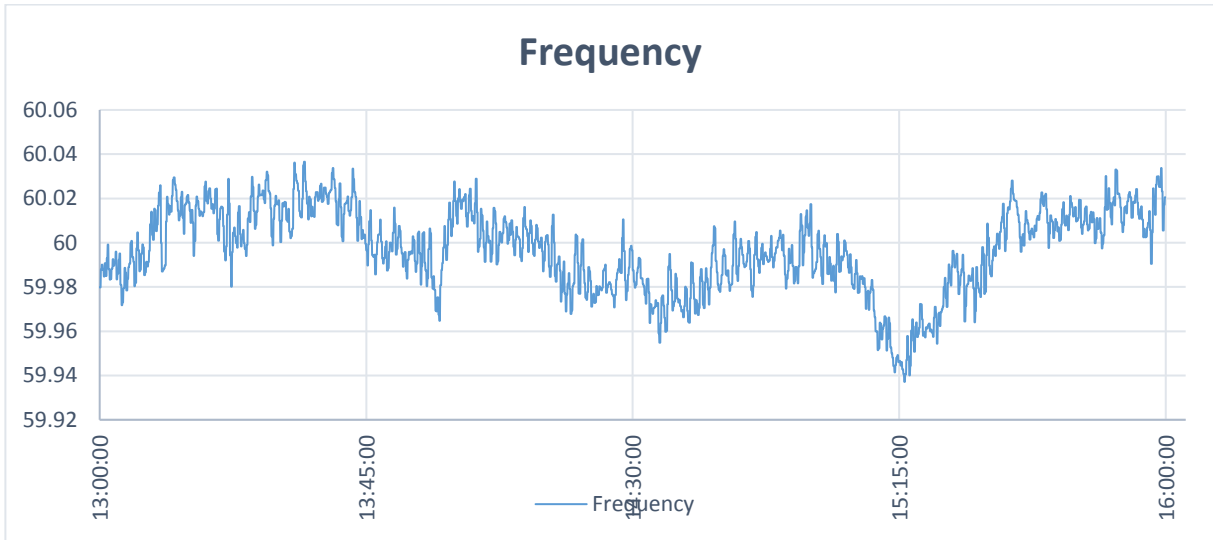


Figure 25: Power System Measurements on March 14, 2017, at 1 pm to 4 pm.

7.5 Torque Measurements

Torque measurements are not required for steady state tests. The shaft of the generator will be at a steady state speed and the requirement to calculate the change in speed of the machine is null. When transient parameters are required, the transient torques on the shaft are required to calculate the change in speed of the shaft.

7.6 Summary

Through the realization of the parameter estimation on a physical laboratory setup, it was found that many factors affect the performance of the filter's ability to estimate parameters. An analysis was made on the sensitivity of the laboratory equipment and the UKF abilities, and it was found that a higher sample rate than 8 kHz such as 30.72 kHz was required for the filter to be stable without requiring engineering judgment to compensate for the error. If the experiment were to be extended into the transient parameters, high sample rates for voltage, current, rotor

angle, and torque measurements must be provided to ensure an accurate calculation for the UKF filter to estimate accurate values.

Chapter 8: Conclusion and Future Scope

8.1 Conclusion

With the advent of the WECC requiring utilities to parameterize machines, the ability to parameterize generation online has become more of interest. The standard for machine parameterization currently is the IEEE 115 standard, which requires the machine to be taken offline to conduct the tests, costing extra time. The purpose of this thesis is to test and prove the ability to parameterize a synchronous machine without taking it offline.

In this thesis approaches to parameterize an online machine were reviewed as well as advice taken from Michael West, the previous researcher on this project. Different approaches such as a black box, gray box, and white box techniques were researched, and it was determined a gray box would yield the best results. Due to the non-linear system behavior of the machine, a nonlinear filter was selected to approximate the parameters. Since the Least Squares Estimation had already been selected by Mike West, the Unscented Kalman filter was selected for this thesis.

This thesis explored the application of the unscented Kalman filter, and a realization of the filter was created in the MATLAB environment for initial testing and calibration. The main testing of the filter was done with the Simulink add-on of MATLAB and tested in the discrete time domain to replicate being implemented in a microcontroller based device. The filter was tested at 8 kHz calibrated after numerous tests to simulate laboratory testing. Once the filter was calibrated, it was tested as if it were in the field by running in real time off discrete data. In both the steady state and transient test cases, the filter could approximate the parameters, which were simulated to be unknown, to within 5% error of the actual value.

To realize the filter on a physical synchronous generator, tests were conducted on the University of Idaho's 20 horsepower generator in Buchannan Engineering Laboratories. Steady state condition tests were gathered, and the operational data was used to characterize the synchronous machine against generator characterization measurements that were conducted before testing. Two steady state test sets were conducted for the characterization of the synchronous machine, as well as determining the performance of the filter. The first test was tested at 8 kHz with an SEL-411L relay which demonstrated that the UFK could characterize L_{md} and L_{mq} of the machine with errors below 3%. However, when testing at 8 kHz using a relative encoder, the data must be post-processed and evaluated with engineering judgment since the resolution of the sample points may lead to errors in the calculations. If the error in the calculation extends beyond one sample point, the filter will become unstable, and L_{ls} will not converge to a specific value due to the set of equations chosen.

The second test set was conducted at 30.72 kHz with an SEL-735 relay primarily because this sample rate was the next higher available sample rate. Due to the higher sample rate, the performance of the filter and the ability to parametrize a synchronous machine increased substantially. The errors for L_{md} and L_{mq} were still around 3%, the same as from the 8 kHz. However, the L_{ls} estimation was around 0.5% error instead of 35%, proving that the filter can parameterize a synchronous machine when it has enough sample resolution.

To realize this algorithm into a fully packaged online estimation device, the sample rate will need to be greater than 8 kHz or an absolute encoder will be needed. The 8 kHz rate which was tested in Simulink was found to be at the edge of the ability to accurately capture the mechanics of the rotor position and A-Phase voltage to parameterize the machine with the laboratory setup. This thesis finds that a higher sample rate such as 30.72 kHz is recommended to characterize

the machine without any additional engineering judgment after the tests have been recorded to allow for automation of the full process.

This thesis has explored methods to parameterize online synchronous machines. The Unscented Kalman Filter was chosen for this process and MATLAB code was produced. The UKF filter was then tested and calibrated with the Simulink environment for both steady state and transient tests. Once the UKF was calibrated, it was used to test a physical laboratory setup at the University of Idaho. The UKF could consistently identify the steady state parameters of an online synchronous generator at 30.72 kHz. However, the UKF had difficulty identifying parameters at 8 kHz due to A-Phase voltage alignment issues. Second, tests have not been conducted to determine the transient parameters of the 20 horsepower synchronous generator since it does not have a feedback loop.

8.2 Future Work

If this online parameter estimation method were to be continued, additional work would need to be produced on the transient parameter estimation. This includes work on the physical laboratory experiment for tuning the AVR and VFD to respond properly when a load is switched onto the system. The generator tested in the simulation was much larger than the one being used in the lab, and could handle a pickup in load without much control. The synchronous generator will be stressed without a tuned AVR and torque control. Additionally, data logging will need to be implemented for the AVR to sample both the field voltage and current. A higher sample rate such as 30.72 kHz should be considered so the filter can capture both sub-transient, and transient conditions and parameters.

Through laboratory testing, it was found that the synchronous generator needs a feedback loop to keep its power factor constant. Further work needs to be done to tune the AVR and VFD

such that it can mimic an online generator. Currently, the ability to reliably calculate the load angle purely depends on whether or not the machine is at the same power factor when a consecutive measurement is made.

Second, additional research will need to be continued in capturing the mechanical rotor angle and the alignment with the A-Phase voltage. At 8 kHz, it was found to be difficult when trying to align the rotor encoder data to the A-Phase voltage peak. The current rotor encoder is the BEI CH05 SSI single turn encoder with 13 bits of resolution. At 8 kHz the BEI encoder samples the rotor every 0.922 degrees, moreover, at 15.36 kHz it samples every 0.48 degrees at 60Hz. Chapter 6 has proven that when the BEI encoder is sampled at 15.36 kHz and re-sampled to 30.72 kHz is sufficient for this application due to the increased number of samples. It has been recommended by others that using one device to record the voltages, currents, and rotor position with an absolute encoder would remove the issues of time alignment and increase accuracy.

A few methods were proposed through academic papers that could be considered to improve rotor angle measurement to improve parameter estimation. The first is using a programmable automation controller (PAC). The PAC had the ability to incorporate GPS time into its measurements of the absolute rotor encoder which uses SSI, and then transfers the data through Ethernet to a central system for calculations. The rotor data can then be time aligned with voltage measurements without any engineering judgement. The second recommended method is through capturing rotor angle with a hall effect encoder which produces analog outputs. These analog outputs can be recorded in a microprocessor based relay which automatically time aligns the voltages, currents, and rotor angle. If a new rotor encoder is to be used it is recommended that an absolute single turn encoder which has a resolution 12 bits or higher.

For laboratory testing, it was noted that when the AVR is in use, the Digilent chipKIT pro MX7 continuously trips rendering all the rotor encoder measurements null for the tests. If the Digilent chipKIT pro MX7 is to be used in further experimentation with the AVR, a guard which protects the device and all cabling from electromagnetic interference will be required. If the rotor encoder is to be replaced with a hall effect sensor and is implemented in a microprocessor based relay this problem would be removed.

Further testing will need to be produced on the transient and subtransient parameters of the 20 horsepower synchronous generator in the laboratory. The transient parameters will first need to be verified through the IEEE 115 standard, and checked against previous measurements on the machine. Once the transient parameters have been found, installation of a feedback loop for both the governor and exciter is recommended to commence these tests. The inclusion of the feedback loop will enable the synchronous machine to stay stable while undergoing a transient condition. Stability factors such as under voltage/frequency and over voltage/frequency will need to be monitored throughout the tests.

Through the implementation of the filter, a few MATLAB scripts were created to automate the UKF for field testing. The UKF itself is set up as a series of modular functions requiring specific inputs which have been commented in the code structure. It is recommended that this filter be implemented in a device which can store or read in all required measurements. The primary consideration of field implementation is how the rotor encoder data is being captured. If a synchronous machine is using a relative encoder, the rotor encoder data will need to be aligned to A-Phase voltage as described in Chapter 6. If it is an absolute encoder, the electrical rotor angle may be analyzed by the filter without alteration with the assumption it has already been aligned to the A-Phase voltage.

References

- [1] “Program Areas & Departments,” *Program Areas & Departments*. [Online]. Available: <http://www.nerc.com/pa/Pages/default.aspx>. [Accessed: 28-Apr-2017].
- [2] *IEEE Guide for Test Procedures for Synchronous Machines Part I Acceptance and Performance Testing Part II Test Procedures and Parameter Determination for Dynamic Analysis, IEEE Std 115-2009 (Revision of IEEE Std 115-1995)*, vol., no., pp.1,219, May 7 2010 doi: 10.1109/IEEESTD.2010.5464495
- [3] M. Ehmer and F. Khan, “A Comparative Study of White Box, Black Box and Grey Box Testing Techniques”, *International Journal of Advanced Computer Science and Applications*, vol. 3, no. 6, 2012.
- [4] Mohd. Ehmer Khan, “Different Approaches to White Box testing Technique for Finding Errors”, *International Journal of Advanced Computer Science and Applications*, Vol. 5, No. 3, pp 1-13, July 2011
- [5] Mohd. Ehmer Khan, “Different Approaches to Black Box Testing Technique for Finding Errors” *International Journal of Advanced Computer Science and Applications*, Vol. 2, No. 4, pp 31-40, October 2011
- [6] M. R. West, *Online Dynamic Parameter Estimation of Synchronous Machines*, MSEE, University of Idaho, 2016.
- [7] T. A. Lipo, *Analysis of synchronous machines*. Boca Raton, FL: Taylor & Francis, 2012.
- [8] Krause, P. C., Wasynczuk, O., Sudhoff, Scott D.; *Analysis of Electric Machinery and Drive Systems*; Second Ed. Wiley-Interscience, 2002. ISBN: 0-4717-14326-X
- [9] A. E. Fitzgerald, C. Kingsley, and S. D. Umans, *Electric machinery*. New York: McGraw-Hill, 2014.
- [10] P. M. Anderson and A.-A. A. Fouad, *Power system control and stability*. New York: Wiley, 2003.
- [11] Chapman, S. J., *Electric Machinery Fundamentals*, Fifth Ed. McGraw-Hill, 2012, ISBN:978-0-07-352954-7
- [12] S J. Julier and J.K. Uhlmann. A New Extension of the Kalman filter to Nonlinear Systems. In Proc. Of Aerosense: The 11th Int. Symp. On Aerospace/Defence Sensing, Simulation and Controls., 1997.
- [13] S. J. Julier J.K. Uhlmann, and H. Durrant-Whyte. “A new approach for filtering non-linear systems.” *In Proceedings of the American Control Conference.*, pages 1628-1632,1995.
- [14] R. van der Merwe, J. F. G. de Freitas, A. Doucet, and E. A Wan. *The Unscented Particle Filter*. Technical Report CUED/F-INFENG/TR 380, Cambridge University Engineering Department, Cambridge, England, August 2000.

- [15] R. van der Merwe and E. A. Wan. “The square-root unscented Kalman filter for state and parameter-estimation”. *To appear in International Conference on Acoustics, Speech, and Signal Processing*, Salt Lake City, Utah, May 2001.
- [16] E. A. Wan and R. van der Merwe. “The Unscented Kalman Filter for Nonlinear Estimation”. In *Proceedings of symposium 2000 on Adaptive Systems for Signal Processing, Communication and Control (AS-SPCC)*, Lake Louise, Alberta, Canada, October 2000 IEEE.
- [17] D. Simon, *Optimal state estimation: Kalman, H_∞ , and nonlinear approaches*. Hoboken, NJ: Wiley, 2006.
- [18] MATLAB and SIMULINK Toolbox Release 2013b, The Mathworks, Inc., Natick, Massachusetts, United States (<http://www.mathworks.com/>)
- [19] S. Mohan, N. Naik, R. M. O. Gemson, and M. R. Ananthasayanam, “Introduction to the Kalman Filter and Tuning its Statistics for Near Optimal Estimates and Cramer Rao Bound,” *Elect. Eng. Indian Institute of Technology, Kanpur*, TR/EE2015/401 February, 2015.
- [20] D. F. Delchamps, *State space and input-output linear systems*. Springer, 2012.
- [21] B. Friedland, *Control system design: an introduction to state-space methods*. Mineola, NY: Dover Publications, 2005.
- [22] E. Ghahremani and I. Kamwa, “Online State Estimation of a Synchronous Generator Using Unscented Kalman Filter From Phasor Measurements Units,” *IEEE Transactions on Energy Conversion*, vol. 26, no. 4, pp. 1099–1108, 2011.
- [23] K. Lin, E. Kyriakides, G. T. Heydt, N. Logic, and B. Singh, “Experience with synchronous generator parameter identification using a Kalman filter,” *IEEE PES General Meeting*, 2010.
- [24] G. Valverde, E. Kyriakides, G. T. Heydt, and V. Terzija, “On-line parameter estimation of saturated synchronous machines,” *2011 IEEE Power and Energy Society General Meeting*, 2011.
- [25] Nasser Tleis, *Power systems modelling and fault analysis theory and practice*. Burlington MA: Newnes, 2008.

Appendix A – Characteristics

Open Circuit Characteristics

Table 22: OCC Characteristics

Test Number	I Field / sqrt(2)	IFD	V12	V23	V31	VOC	VLN
1	1.576848122	2.23	170	170	170	170	98.14955
2	1.71119841	2.42	180	180	180	180	103.923
3	1.838477631	2.6	190	190	190	190	109.6966
4	1.97282792	2.79	200	200	200	200	115.4701
5	2.107178208	2.98	210	210	210	210	121.2436
6	2.248599564	3.18	220	220	220	220	127.0171
7	2.382949853	3.37	230	230	230	230	132.7906
8	2.538513344	3.59	240	240	240	240	138.5641
9	2.708218972	3.83	250	250	250	250	144.3376
10	2.856711396	4.04	260	260	260	260	150.1111
11	3.040559159	4.3	270	270	270	270	155.8846
12	3.224406922	4.56	280	280	280	280	161.6581
13	3.422396821	4.84	290	290	290	290	167.4316

Table 23: Calculated Xd Values

Test Case	X_d
1	4.121855
2	4.021664
3	3.951199
4	3.875917
5	3.810234
6	3.740625
7	3.690172
8	3.614643
9	3.529311
10	3.479691
11	3.395033
12	3.320029
13	3.239674

Synchronous Condenser Operation to Calculate X_q Data

Table 24: Synchronous Condenser Operation

Test Number	I1	I2	I3	IL	V12	V23	V31	I_{fgen}	V_{fgen}
1	16.4	16.4	16.4	16.4	220	220	220	1.98	35.2
2	9.93	9.97	9.88	9.92666	220	220	220	2.46	43.5
3	13.07	13.03	13.05	13.05	220	220	220	2.21	39.2
4	6.87	6.9	6.83	6.86666	220	220	220	2.69	47.5

Table 25: Calculated X_q Values

Test Number	X_q (ohm)
1	2.8623
2	2.9424
3	3.0285
4	2.9978

Appendix B – AMPS Setup

Variable Frequency Drive

ACS550

Encoder

BEI CHO5 SSI Absolute Single Turn Encoder

Current Transformer

SEL-411L Relay Settings

General Settings

CTR - 30

PTR – 1

Trip Logic

TR – PB7_LED

Outputs

Interface Board Outputs

OUT201 Interface Board 1 Output OUT201 (SELogic) – PB7_LED

Report

Event Reporting

SRATE – 8

LER – 0.25

PRE – 0.05

Event Reporting Analog Quantities

VAYFM

VBYFM

VCYFM

IAWFI

IBWFI

ICWFI

FREQPM

3PF

FREQP

SEL-735 Relay Settings

General Settings

CTR - 30

PTR – 1

Trip Logic

TR – OUT101

Event Report

ER1 Event Report Equation 1 – PB03

SRATE - 512

LER - 120

PRE - 1

EVE_SCA – PRI

Inputs/Outputs

OUT101 – FAULT OR PB03

Analog Model Power System

Synchronization to the Power Grid

To connect the synchronous generator to the grid the following steps will need to be followed:

1. First, begin by making sure all the breakers are open on the AMPS system
2. Next start with connecting the synchronous generator to the terminal box behind the VFD

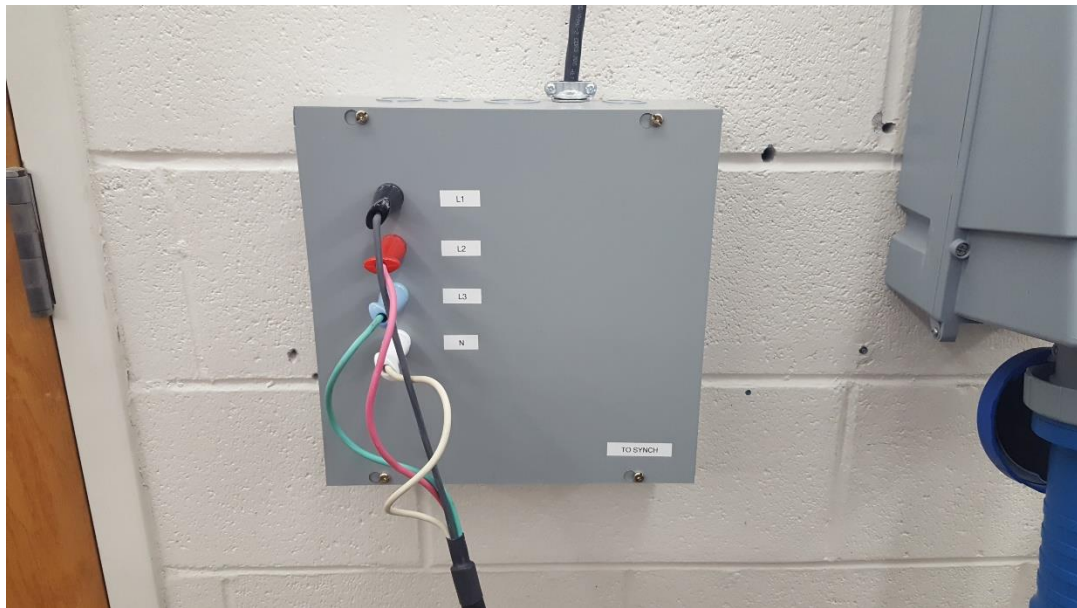


Figure 26: Connection Panel next to 20 hp Synchronous Generator

3. The panel in step 2 connects the generator to the AMPS distribution panel seen in Figure 27. Take the “longest” lab cables and connect them to bus 22 on the AMPS system as noted in Figure 28. There is an additional connection from bus 23 to bus 24. This is because the Synchroscope is connected to bus 24. The Synchronous generator must be connected to bus 24 via bus 22. This is a radial system as seen by disconnecting bus 37 or 38 from the system.



Figure 27: Connection Panel On AMPS System Above Computer

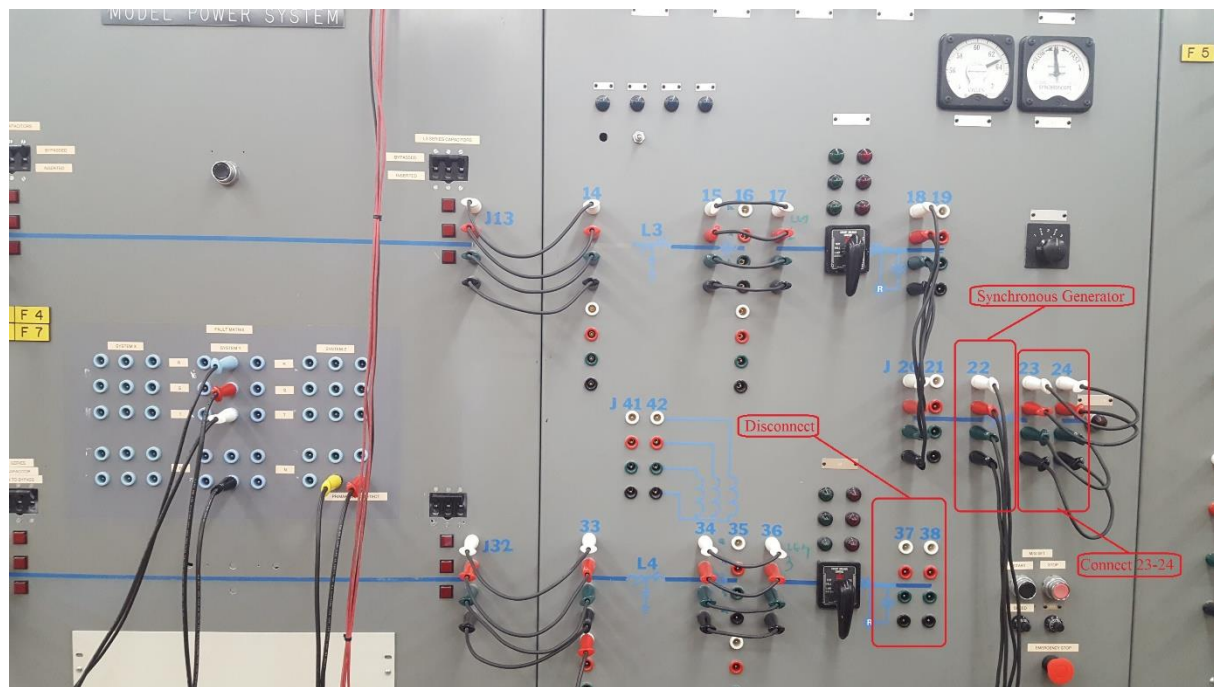


Figure 28: Generator Bus Configuration

4. Before starting the generator, it is important to make sure the AMPS M/G set is disconnected via the breaker box as seen in Figure 29.



Figure 29: Breaker Box for AMPS MG set

5. After the generator, has been connected, and the AMPS MG set has been disconnected, turn on the AMPS system.
6. Bring the generator up to rated speed and up to the AMPS voltage. This will be around 208V to 215V Line-to-Line depending on the grid voltage.
7. Close Breaker 1 on the AMPS system.
8. Figure 30 shows the synchroscope located next to the generator bus on the AMPS system. This should be spinning, if it is not turn off the system and check the system is connected properly. If it is, make sure it is spinning counter clockwise, meaning slightly above rated frequency. This ensures the generator will export power when synchronizing to

the grid, not importing power. If the machine is not above rated frequency, adjust the VFD such that it says 60.1 Hz on the face plate.



Figure 30: Synchroscope

9. The best time to synchronize the generator is when the needle is about 10 degrees from the vertical position. This ensures the minimal power export and minimum torque on the generator. When ready, turn the Breaker 2 handle clockwise as fast as possible to sync the generator.